2019-01-01

Numerical Investigation Of Molten Metal Infiltration And Pillared Cooling Systems At Microscale

Shaikh Tanveer Tanveer Hossain
University of Texas at El Paso

NUMERICAL INVESTIGATION OF MOLTEN METAL INFILTRATION AND PILLARED COOLING SYSTEMS AT MICROSCALE

SHAIKH TANVEER HOSSAIN

MASTER'S PROGRAM IN COMPUTATIONAL SCIENCE

APPROVED:

Vinod Kumar, Ph.D.

Vivek Tandon, Ph.D.

Xianyi Zeng, Ph.D.

Stephen Crites, Ph.D.
Dean of the Grad

DEDICATION

To my mother, Noor Jahan Khatoon

NUMERICAL INVESTIGATION OF MOLTEN METAL INFILTRATION AND PILLARED COOLING SYSTEMS AT MICROSCALE

by

SHAIKH TANVEER HOSSAIN

THESIS

Presented to the Faculty of the Graduate School of

The University of Texas at El Paso

in Partial Fulfillment

of the Requirements

for the Degree of

MASTER OF SCIENCE

Computational Science Program

THE UNIVERSITY OF TEXAS AT EL PASO

August 2019

ACKNOWLEDGEMENT

I want to express my heartfelt gratitude and appreciation to my mentor Dr. Vinod Kumar for his continuous support, guidance, and belief in my research work. I want to thank my committee members Dr. Xianyi Zeng and Dr. Vivek Tandon for their wonderful gesture, support, and for reviewing my thesis paper.

Special thanks go to the Department of Computational Science for giving me teaching assistantship support throughout my graduate study. My special gratitude to Dr. Ming-Ying Leung and Dr. Kumar for understanding my struggle with my chronic sickness since 2016 and helping me to get treatment while continuing my study. I want to thank Dr. Kumar for teaching me the basics of fluid dynamics simulation for pours medium which helped me to get interested in working on that field. I want to thank Dr. Kumar's research group members Mr. Ashesh Chattopadhyay, Mr. Arturo Shafino, Mr. Arturo Rodriguez and Dr. Murali. I want to especially thank Ashes Chattopadhyay whose continuous effort helped me to understand the background of this work and to continue the work till the end. Also, thanks to Dr. Zeng, Dr. Moor, Dr. Leung and Dr. Sewell for teaching me parallel computing and HPC which is one of the basic things needed for this thesis. Also, I want to express my gratitude to Mrs. Cindy (Co-Ordinator of Computational Science till spring 2018) for her motherly affection and supports.

I am thankful to my girlfriend, my love, Tahmina Tanni, to stand beside me in my crisis moments. Her continuous support was crucial to complete my work when I was sick. I am wholeheartedly thankful to my friend Rahat and Shimanto for being there for me. I am grateful to my neighbors and other friends for helping me on several issues.

My kindest gratitude and thanks go to my family for allowing me to come to a foreign country to go to graduate school. I am grateful to my uncles, aunts, grandfather, and to my father and mother for all their teaching to be a good human being to live peacefully by helping others.

Finally, I would like to thank the University of Texas at El Paso College of Science, the Graduate School, for their support.

ABSTRACT

Flow-through porous media at pore-scales is one of the less explored sides of fluid mechanics due to the complexity associated with highly irregular pore geometry. Most of the established methods that try to quantify such flow are based on statistical observations of flow through numerous porous specimens. Such understandings may satisfy the need for applications where micro-level details are not a concern. Some numerical approaches did try to analyze the micro-level flow, but the analysis was confined to small sample sizes due to the intensive computation challenge. There are several applications of porous media flow where analyzing the large-scale flow physics combined with the micro-level details can make a big difference. For example, the flow of molten metal through a matrix when manufacturing Metal Matrix Composites and flow of water through a micro-pillared cooling system.

In this thesis, I used the pore network flow analysis software - Exascale Pore Network Simulator or EXPNS – an in-house software developed by our research group. The software is based on the "network resistance theory" for the molten metal flow through an irregular shaped matrix and Sandia's scalable and portable software framework, and hence is uniquely designed to harnesses the power of high-performance computing (HPC) and can handle data- and computation-intensive problems. Metal Matrix Composites are on high demand in the car and aerospace industry due to its desirable properties; this flow analysis will help to increase products quality. Besides this, I also analyzed flow resistances of the flow-through micro-pillared wick structure with variable diameter, relevant for understanding the heat removal bottleneck in the electronic chip. Capillary-based micro-pillared wick structure cooling system is a promising new solution for that. I analyzed the flow resistances of such structures with variable diameter which can help better understand the flow.

TABLE OF CONTENTS

LIST OF FIGURES

CHAPTER 1: INTRODUCTION

This chapter introduces the reader about each of the upcoming chapters and gives a brief description of the material in that chapter. In this work, we modeled two different types of porous flow case, which have a similar underlying structure.

Chapter two describes the earlier works and concept related to this thesis. This Chapter two is divided into 5 bold divisions. The 1st one describes the high-performance computing system and its necessity and benefits. The work done in this thesis is entirely dependent on high-performance computing facilities. The work here modeled porous media while keeping in considering details of its micro-structure level flow physics. This poses a massive data and computation intensive calculation challenge. To overcome that the application of high-performance computing is not a beneficial tool rather a necessity. The 1st portion of chapter 2 is so dedicated to the concept regarding high-performance computing and describes the exascale preformation benefits.

In chapter 2.2 it describes the heat management challenges faced by the manufactures and scientists for the ever-shrinking and power-hungry electronics devices like computer chips/ processors. While higher speed computer chips are in continuous demand, on the other hand, it is not possible to achieve more high-speed chips due to lacking materials that can operate at a higher temperature. Chapter 2.2 describes these and many cooling solutions along with it and their advantages and disadvantages.

In chapter 2.3, the working principle of thin-film-evaporation is described. Thin-film evaporation is one of the most advantageous and efficient heat removal process discussed in chapter 2.2. We in this thesis tried to evaluate the resistance of the flow-through these micro pillared thin film

evaporation systems so that its flow can be modeled for better understanding and enhancing the heat transfer.

In the chapter, 2.4 Matrix Metal Composites are introduced. Matrix Metal composite is one of the promising materials getting used in these days from car manufacturing to space shuttles construction. Production of these matrix metal composites needs flow of molten metal through ceramic or other porous media. Understanding this flow is very important as the improper flow can contribute to low-quality products. In this work, this flow is modeled and analyzed.

In chapter 2.5, a brief description of an algorithm which is used to model the above two problems named Exascale pore network simulator (EXPNS) is described. EXPNS is a pore network simulator developed on network resistance modeling technique of electronic circuits and used here for modeling molten metal flow through a matrix structure.

In Chapter 3, The two problems that we are working on in this thesis is described. One of them is the flow analysis through the porous matrix, and another one is finding the resistances of flow through the micro-pillared thin-film cooling system. It also describes the previous works and progresses happened in these sectors and how our works will differ from the earlier works.

Chapter 4 is for methodology- it describes the techniques we used to solve these problems. The 1st section of this chapter is dedicated to the description of the EXPNS working principle which was developed by our research group to simulate flow through a porous medium. Then in chapter 4.2 a validation of that algorithm was given which gives the credibility of the next step's works which is modeling with that algorithm. Then the next two chapters give an elaborate description of how the flow-through matrix was modeled with the EXPNS and how the resistances of flow through micro-pillared thin-film evaporation system was done with the help of Solidworks and Anasys.

Chapter five describes the results from the two works and the results from the validation part. For the molten metal flow graphs showing penetration depth vs. time and penetration rate vs time was shown. For the other work, the resistances for different combinations of structures was given.

In the end, in chapter six, a summary of the work is given with possible future work scope and utilization.

A list of to the all the citing in writing could be found at the end in the reference chapter.

CHAPTER 2: BACKGROUND AND LITERATURE REVIEW

2.1 HIGH-PERFORMANCE COMPUTING:

The current age is known as the age of information. With the very recent advancement in the digital storage system, it is now very cheap to store a massive amount of data. Also, a vast improvement happened in computing technology, which is allowing the handling of these data at a high-speed rate. As a result, a lot of physical problems, business analytical problems and many other problems which was impossible to attempt previously due to lack of computing technology are now being aimed.

High-performance computing or HPC, in short, refers to the computing facility that can work very fast with a huge amount of data and provide a vast amount of computing speed. Usually, an HPC can perform hundreds of quadrillions (10^{15}) calculations (flops) per second [1]. The typical example of this facilities are supercomputers; where thousands of compute nodes works in parallel to solve a task and hence have a thousand times more computing speed than an individual home computer. Day by day, the application of HPC is increasing because of its prospectus in groundbreaking research and game-changing innovations.

The largest user of High-performance Computing is Computational fluid dynamics [2]. It has been used for greater understanding of turbulence, heat and mass transfer in engineering applications, Industrial flow, and combustion system, flow in river and channels, flow through porous media, weather prediction, and many others. Direct numerical simulation, where the Navier-stokes equations are solved numerically for the whole range of spatial and temporal scales of the turbulence is typically the most computation power consuming. It was found that the computational resources required increases approximately with the third power of Reynolds

number [3]. Moreover, most of the Industrial flow or flow around an aircraft are highly turbulent-which implies a high Reynolds number. To reduce the computing resource needed, different turbulence models and schemes have always been used. However, still, a large size of matrixes is typically required to be solved for these problems. To address these with traditional serial algorithms even using a single processor of highest computing speed may take years of computing time. Besides, it is very often that the data needed to be kept in the DRAM is too much higher to store in a single processors DRAM. So, dividing the problem into smaller sub problems and then solve simultaneously by a cluster of processors (supercomputer) is inevitably the solution. And that is parallel processing and high-performance computing all about.

Some terminologies related to High-Performance Computing is described below:

2.1.1 Distributed Computing Message Passing Interface (MPI)

In the distributed memory computing system, Individual processors have separate memory space, and they are connected by a network. The Message Passing Interface Standard is such a library standard developed by a group of researchers from academia and industry for various parallel computing architectures. The target of the MPI is to offer a portable, efficient, and flexible standard for message passing that will widely use for writing message-passing programs [4]. In MPI the computational task is divided amongst various processors which perform their own tasks and returns the result to a single processor to be assimilated. The processors can communicate either point to point or collectively. MPI has become the *de facto standard* for communication among processors in a parallel code which uses a distributed memory system [5].

A problem that can be sub-divided into n numbers of problems can be theoretically n times faster. However, most of the problems are not “embarrassingly” parallel and so a serial part always stays

inside the code. The time needed for computation as a function of the number of processors is stated by Amdahl's Law as [6] [7] :

$$S_{Latency} = \frac{1}{(1-p) + {}^{p}/_{s}} \qquad \textit{Eqn:1}$$

Where, $S_{Latency}$ is the amount of speed up, p is the fraction of serial runtime of the code which could be parallelized and s is a factor at which the parallel portion will be accelerated. It is evident from the equation (1) that even if we have infinite number processors, the serial part will remain the same.

On the other hand, computer scientist John L. Gustafson states another rule for calculating the speed up, which is [8]:

$$S_p = F_s + PF_p = P - (P-1)F_s \qquad \textit{Eqn:2}$$

Here, p is the number of processors, F_s is the serial fraction and S_p is the speedup. According to this formula, the speedup will increase linearly. He argued that when the number of processors will increase the scientists will increase their datasets or expand parameters to get more accurate results. However, none of the above cases assumes that any processors will be needed data from others and hence will add slack time. In general, for a complex code the formula used is:

$$S_p = \frac{T_s}{T_p} = \frac{1}{F_s + \frac{F_p}{P} + T_c} \qquad \textit{Eqn:3}$$

Here, T_c is the overhead time taken between processors.

MPI is one of the most used distributed memory-based parallel processing libraries. In this thesis, MPICH is used [9]. Most of the cases, the MPI is not used directly in our case. Instead, Trillions (a collection of open-source scientific software libraries) is used.

2.1.2 Communication Topologies Of MPI:

It is prevalent to exchange data between processors for a parallel code run. It helps to distribute the load equally. On the other hand, increasing node numbers results in increased communication time. So, it is very vital to understand the virtual architecture of the nodes/ processors. A linear array or ring topology, mesh topology, and the hypercube is the most prominently used topologies [10] [4]. The linear array or ring topology is the simplest one. It is logically assembled as a row and wrapping at the end makes it a ring. The mesh topology arranges them is a cartesian grid with or without any wraparound. The grid could be 2D or 3D. It is usually expressed as a $n - D\ k$ array where n indicates the number of dimensions and k suggests the number of processors in each dimension. In hypercube topology, it is a d dimensional mesh where $d = logp$. Here, p is the number of processors. In this case, any node i is linked to its j neighbors differing by one bit in its address. Based on this connectivity difference, the run time of a parallel algorithm varies. The distance between two farthest nodes in a topology is called the diameter of that topology. Another critical term to determine the communication bottleneck is bisection width. Bisection width is the minimal number of links to be cut of network architecture to make it two independent equal sizes (plus or minus one) topology [11]. Besides these, there are many other kinds of topologies [12], all of which is out of the scope of this thesis work. Table 1 shows the communication costs, diameter, and bisection width for different topologies.

Besides these point to point communication, also there are one to all (send data form all the processors), all to one (collects data from all the processors and send to one) and all to all (where everyone gets the full sets of data) communication process.

All this communication process differs in communication time with the variance in topology. For a single communication, the formula is [13]:

$$T_{comm} = T_i + T_m \qquad \textit{Eqn:4}$$

Here, T_i is the set-up time to initialize a communication time and T_m is the time needed to send a message of length m. So, it can be written as,

$$T_{comm} = T_i + {}^{m}/_{B} \qquad \textit{Eqn:5}$$

B is the bandwidth. In cases of, n number of messages it will be

$$T_{comm} = n * (T_i + {}^{m}/_{B}) \qquad \textit{Eqn:6}$$

Using this basic formulation, the theoretical communication cost of all to all communication for (a) linear array/ ring topology (b) 2D mesh (c) Hypercube is derived as [14] [15]:

(a) $$T_{comm,ring/linear} = (T_i + m * T_m) * (P - 1) \qquad \textit{Eqn:7}$$

(b) $$T_{comm,2D\ mesh} = 2T_i\left(\sqrt{P} - 1\right) + m * T_m * (P - 1) \qquad \textit{Eqn:8}$$

(c) $$T_{comm,Hypercube} = \sum_{i=1}^{\log(P)} (T_i + 2^i * T_m * m) = T_i * \log(p) + T_m * m * (P - 1) \qquad \textit{Eqn:9}$$

Where P indicates the number of processors. Depending on the communication needed, the available number of processors and communication type, the topologies are created.

Table 1: Networks topologies with their parameters

Network	Diameter	Bisection Width	Cost (Number of Links)
Completely Connected	1	$\frac{P^2}{4}$	$P(P-1)$
Complete Binary Tree	$2\log\left(\frac{P+1}{2}\right)$	1	$(P-1)$
Linear Array	$(P-1)$	1	$(P-1)$
2-D mesh no wraparound	$2(\sqrt{P}-1)$	$\sqrt{P}$	$2(\mathrm{P}-\sqrt{P})$
2-D mesh with wraparound	$2[\frac{\sqrt{P}}{2}]$	$2\sqrt{P}$	$2P$
Hypercube	$\log P$	$\frac{P}{2}$	$\frac{P\log P}{2}$

2.1.3 Shared Memory Based Computing:

In the shared memory-based computing algorithm, processors in a single node have Uniform Memory Access (UMA); has shared memory and have access at equal priority and rate. In Non-Uniform-Memory-access system, each processor contains one memory stick and have faster memory access to its own stick [16] [17]. Although all the memory sticks are accessible by all the cores [18]. So, in that case, the programs are designed in such a way that the memory needed for one processor stay in its memory stick. In this way, it can achieve more speed up than a traditional UMA system. Most modern computers, especially the ones working on scientific calculations, uses NUMA structure.

The most used shared-memory-based parallel computing model is Open MPI. Open MPI is an API supported by C, C++, and Fortran that implements directive-based parallel programming [19].

Though Open Mpi was not used directly in this thesis, instead, Kokos was used which implement Open Mpi. Kokos is C++ Library which makes a parallel code portable [20].

Another shared memory-based API which used the Graphics Processing Unit (GPU) is called CUDA. Previously, the GPU unit was only limited to graphics processing. Only recently, GPU is also getting used for high-performance computing. The GPU architecture is built with shared memory and have hundreds of threads which only can perform the lightweight operation. If the algorithm has parts that can be parallelized over hundreds of lightweight calculations, then using GPU can show a remarkable speedup. Usually, the memory in the CPU is copied to the GPU, and then the CPU works simultaneously. After the GPU work is done it is feedbacked the host (CPU). In this thesis, Kokos was used, which includes the uses of GPU unit.

2.1.4 Hybrid-Parallel Computing Techniques:

Two different types of parallel programming have its merits and demerits. Typically, MPI is good to handle large size programs, especially if the memory required is high. Adding a new node also add new memory in total and hence increase the capability. However, it also increases the communications and required communication and waiting time as well.

On the other hand, OpenMP is useful if no communication is not needed and each processors work is mostly restricted with a unique set of data. In the case of OpenMP, there is a risk of data racing. CUDA is very good at speeding up at a minimal cost. However, CUDA threads can only handle lightweight operations and thus only can be used for specific cases. Also, if the data exchange is much between CPU and GPU, the PCI Bus speed may hamper the speed up a lot.

In the case of hybrid parallel computing, all the penalization models are used in combined while keeping in mind their differences, advantages, and disadvantages. Usually, the main program

is dispatched to MPI threads. Then inside each MPI threads, OpenMP or CUDA threads are created for secondary parallelism. If the combination can be done wisely, then several times speed up can be gained compared to the application of any single method.

2.1.5 Shifting To Exascale :

Exascale computing refers to a computation speed of 10^8 floating-point operations per second. It is not only a hardware challenge but also a software challenge, too [21]. Although not every problem requires exascale capability, the number of problems that demand higher computation speed is on the way of increase. Fields like climate modeling, turbulence, combustion, fluidized bed reactors and porous flow processes are multi-scale problems that get benefited from exascale systems. In this thesis Trilions (a linear algebra library developed by Sandia National Laboratory) is used extremely through APIs developed, which is exascale cable and optimized for communication and parallelism so that it can handle large scale problems. With these the fluid flow physics in a porous media can be understood better.

2.2 HEAT MANAGEMENT CHALLENGE IN ELECTRONICS:

The development trend of electronics in the last couple of decades predicts a continuous increase in power consumption. Mostly this increment of high-power consumption is due to the steady rising of the clock speed of microprocessors. Also, Gan power electronics and telecom devices present a similar heat management challenge. A popularly accepted and long observed trend was predicted by Moore's Law (named after Intel co-founder Gordon E. Moore) which states that the number of transistors on an affordable CPU would double every two years [22]. Which technically implies twice the heat management challenge in every two years.

On the other hand, consumer electronics (Laptop, TV, cell phone, etc.) are decreasing in volume every year. This results in higher heat density. A recent study shows that in contemporary time, an average everyday consumer electronics has a rate of heat generation anywhere between 57 w/cm^2 to 108 w/cm^2 [23]. Without proper management, for this heat removal, it will exceed the allowable operating temperature. A recent market survey of an electronics company showed that the cooling of PC's and telecom electronics has a worth of $4.1 billion per year with an estimated prospect of $4.8 billion in the near future[24]. This study also indicates a large scale shifting from traditional fan cooling to superior technologies for most of the PC and telecom electronics cooling. In electronics, the critical temperature is usually the junction temperature of semiconductors or transistors, which is generally higher than the case temperature. This junction temperature is directly related to power dissipation, thermal resistance, and ambient temperature. Where the function of a heat sink is to provide the lowest possible thermal resistance between the junction and its environment when assuming that the environment is always cooler [25]. The maximum allowable temperature for a semiconductor junction usually varies between 150^o Celsius to 175^o Celsius. Considered the ambient temperature as 25^0 degree Celsius the maximum permissible

increase could be restricted between 125 to 150 degree Celsius. Below this threshold, elevated junction temperature has little effect on the life of a part, but above that threshold, component life shortens exponentially with increasing temperature. However, in the real case scenario, the permissible temperature is much less than this as it must count some safety. Also, the life of the electronic IC's is inversely proportional to the operating temperature so in practice to ensure reliability and cost efficiency the operating temperature is usually kept somewhere near 125^{o} Celsius. Besides these increments of temperature may also produce thermal stress and failure to manage that may lead to a shorter lifetime by mechanical failure. To ensure the convenient temperature a proper heat management system is not an option but essential for the device.

Several cooling systems are used in practice, and some are on the process of development for heat removal from these electronics. Depending on the pros and cons of a cooling system, costing, limitations, and operating conditions of the device, an engineer or product designer have to choose the most suitable one.

2.2.1 Free Convection (Air):

For cases of very low heat generation, it is relatively easy to design. Free convection is utilized mostly in those cases. Some heat spreaders, fins or heat sinks are installed in proper places to transfer the heat to the air. Sometimes heat-conducting adhesives also facilitate the operation. Use of these types of cooling may be widely seen in the simplest electronics where heat is not a much issue to worry about.

2.2.2 Forced Convection (Air):

For low heat generation cases like home electronics and the devices that are not very compact forced convection by the cooling fan is a widely used option. Besides, heat spreaders or heat sinks also used to facilitate the process. In the case of vacuum, some other conducting material and spreaders are used to make a path for heat transfer. However, application of these mechanical based forced convection systems is limited to low heat generating non-compact devices. Also, sometimes this type of cooling method conveys dust particle to the device and could make harm to the device. Example of these is mostly non-sophisticated home and some pocket appliances. In some cases, series installation of the more than one fan is used to push the benefit a little bit further.

2.2.3 Liquid Cooling (Forced Convection):

In cases, where air cooling is inefficient liquid cooling can be used to stretch the limit one step further. Liquid cooling is a hydraulic circuit which transfers heat from heat source to cold place. In cases of low to medium heat management challenge, this can be a good option. However, they draw higher operating energy and needed complicated piping inside the device. Sometimes this may increase the device volume due to its size. With the increment of the load to manage the volume of this system is needed to increase, which increases operating cost and maintenance cost. Also, weight and risk of licking are two of its major disadvantages.

2.2.4 Phase Change Material:

The concept of Phase Change Material (PCM) is relatively new for electronics cooling. Mostly they are applied for the telecom-related electronics. This type of cooling is installed for peak load or overload scenarios. PCM is a material that has a high latent heat of phase change with a suitable melting point. The material is chosen based on the estimated temperature rise or the limiting temperature. There are a lot of PCM materials or system available. The simplest example could be ice/ water system. However, due to having a low melting point of ice, it is not much suitable for most of the electronics. Organic materials like paraffin or wax are mostly used PCMs now. Besides these, a unique solid to solid PCMs are also available to go through a solid/solid phase transition by heat absorption. In case of overload or out of control situation, the heat is absorbed by the melting process of the PCM. When the device comes back to its normal temperature or ambient temperature, the PCM again comes back to solid-state and get ready to serve heat for the next case of overheating. The PCM Materials are kept inside smaller packs and then these packs are installed around the hot spots. Sometimes fins or a heat exchanger is used to facilitate the process. Even though this system has some significant advantages like zero maintenance and high heat removal capacity, but this system does not work where the heat is needed to remove continuously. So, the application is very limited to the devices which are not used consistently, or they are reserved for an overload/ peak load case where a primary heat management system works to handle the regular situation.

2.2.5 Synthetic Jet Cooling:

Synthetic jet cooling is a relatively new technology inspired by the working method of mammal lung. In this technology, a periodic motion of a diaphragm creates a periodic suction and ejection of fluid (usually air) through an orifice bounded by a cavity.[26] By the fast ejection of the air in the ambient air, a vortex is created with a forward motion. Once when the vortex is moved towards the downstream, the suction phase is started. This is like the way we breathe in and breathe out. No external fluid is needed for this procedure. This periodic motion can be created by using different methods like piezoelectric, electromagnetic, electrostatic and combustion-driven pistons. Piezoelectric ones have the advantage of being low weight and low power consumption was the electromagnetic ones are better for noise and reliable performance. Due to their smaller size, this technology gives the designer much freedom compared to other technologies like water cooling. Even though it seems a very cool ultramodern technology, the performance of the system is not that much outstanding. It is somewhat better than the fan-based forced cooling method and is only applicable to a small region with relatively less heat generation.

2.2.6 Heat Pipe:

The heat pipe is a cooling device that applies the process of heat conduction and phase change. Usually, the system is made by a high conductive material (e.g., copper) pipe which goes around the hot body and cooling interface. The tube contains any liquid with the high latent heat of vaporization and a boiling point, less than the desired temperature of the hot body. The heat from the source conducted inside the pipe through the superconductive pipe material and vaporizes the liquid. This vapor then travels through the pipe to the part near the cold surface and reject the latent heat there to become liquid again. This liquid travel back to the heating zone again using capillary action, centrifugal force or gravity and thus completes a cycle. This system is very effective as it

has a high heat removal rate as it uses the latent heat of the liquid. This is basically an example of passive cooling where another cooling system is needed to maintain the low temperature of the cold surface. In the case of electronics, capillary-based heat pipes are mostly used due to their reliability and zero external power consumption. A wick structure is used inside the pipe to carry the condensed liquid to the evaporation zone. This highly efficient system can handle a heat load of 100W-200W with distance up to 300 mm. Low cost and zero maintenance are also two great qualities of this system. The main disadvantage is that it needed a second cooling method for the condenser, which adds operating cost, maintenance and takes space. Also, to handle more heat load, increasing the cross-section nullify to the advantage of capillary action.[27] To overcome that situation, micro-pumps are installed in the circuit, which makes it relatively unreliable and power-consuming sometimes.

2.2.7 Mini Refrigeration System For Electronic Cooling:

Air conditioning or refrigeration system is an early system to lower the temperature of a space. However, usually, this system is used for mostly control room temperature or food and drug preservation. Due to their larger size, they are not suitable for electronics cooling. However, some attempts to make a miniature refrigeration system for electronic cooling has been taken. Just like a traditional full-scale refrigerator, the construction of a miniature refrigerator includes an evaporator, a compressor, a capillary tube, and a condenser. The experimental mini-refrigerators showed a functional heat removal capacity, which is around 200 W [28]. The volume of these experimental devices is approximately $300 \times 230 \times 70$ mm^3. For cooling compact electronics this size is too big and so cannot meet the rising demand.

2.2.8 Spray Evaporative Cooling:

Spray evaporative cooling is a rare used for a small system. Mostly they are used for large size electronics cooling. Water or some other high latent heat liquid is sprayed through a nozzle using a high-power compressor. This sprayed liquid gets evaporated, consuming latent heat from the chip surface and make it cool. This procedure gives a high rate of heat removal. The main reason not to use it in a compact electronics system is the compressor takes a lot of space. Also, due to the high power consumed by the compressor and a continuous supply of cooling liquid is needed, this system is not suitable for smaller electronics cooling.

2.2.9 Thin-Film Evaporation Cooling:

Thin-film evaporation is one of the best cooling technologies with the highest cooling rate in minimal space. This method works by installing a wick structure on the top surface of the chip/ processors, which is connected to a cooling liquid reservoir. The liquid is carried to the wick structure due to capillary action and gets evaporated there taking the heat from the heated body. Multiple factors contribute to this effectiveness. As the heat is removed by a very thin layer of liquid. As a result, the heat transfer coefficient is very high. The removal process uses the latent heat of vaporization, which contributes to high heat flux. As the film is very thin, only a little cooling liquid is required. Due to the capillary action, the liquid is supplied continuously, and they get evaporated almost immediately. So, in this way the heating surface can be maintained at a little higher temperature than the evaporation temperature of the liquid. Effectiveness of this system has already drawn a lot of attention from industry and academic research. Besides recent advances in Nano/ microfabrication technology showed a new opportunity in this filed [29]. There is a lot of

characteristically different type of thin-film evaporator mainly because of the geometry of their wick structure and their arrangement. In this work, we numerically analyzed one of the best-proven geometry for providing the highest heat flux with an additional parameter (non-uniformity of geometry) to estimate and a more real-life scenario of the system's performance.

2.3 THE WORKING PRINCIPLE OF THIN FILM EVAPORATION:

Thin-film evaporation for cooling uses a microfabricated wick structure to draw the cooling liquid for filling up the void space left by the evaporation. The wick structure is installed on the heating surface and is connected to a water reservoir in one or all the side. The wick structure could be made of the micro-sized pillar of any geometry like spherical, cube-shaped, rectangular or cylinder. The construction material is needed to be one with high heat conductivity, unreactive to the cooling fluid and has good capillary attraction force to the working fluid. Also, lightweight and low cost are preferable. Copper, aluminum alloys, silicon are some of the famous examples. The working fluid is chosen based on its boiling temperature and latent heat of vaporization. Also, un-reactiveness to the wick material and having the strong adhesive force to the wick material is needed. In most of the cases, water is a common choice due to its high latent heat of vaporization and availability. The shape of the micropillar structure is significant because these wick pillars create the capillary pumping effect due to its geometrical shape. Experiments have done to find out the characteristics of different regular geometries like a sphere, pyramids, conical, and cylindrical shape [30] [31] [32]. Among them, the cylindrical shaped was to be found the most efficient [31]. More efforts to find out the optimum diameter, pitch and height of the cylinders in the cylinder based wick structures are also done [32] [33] [34] [29][35].

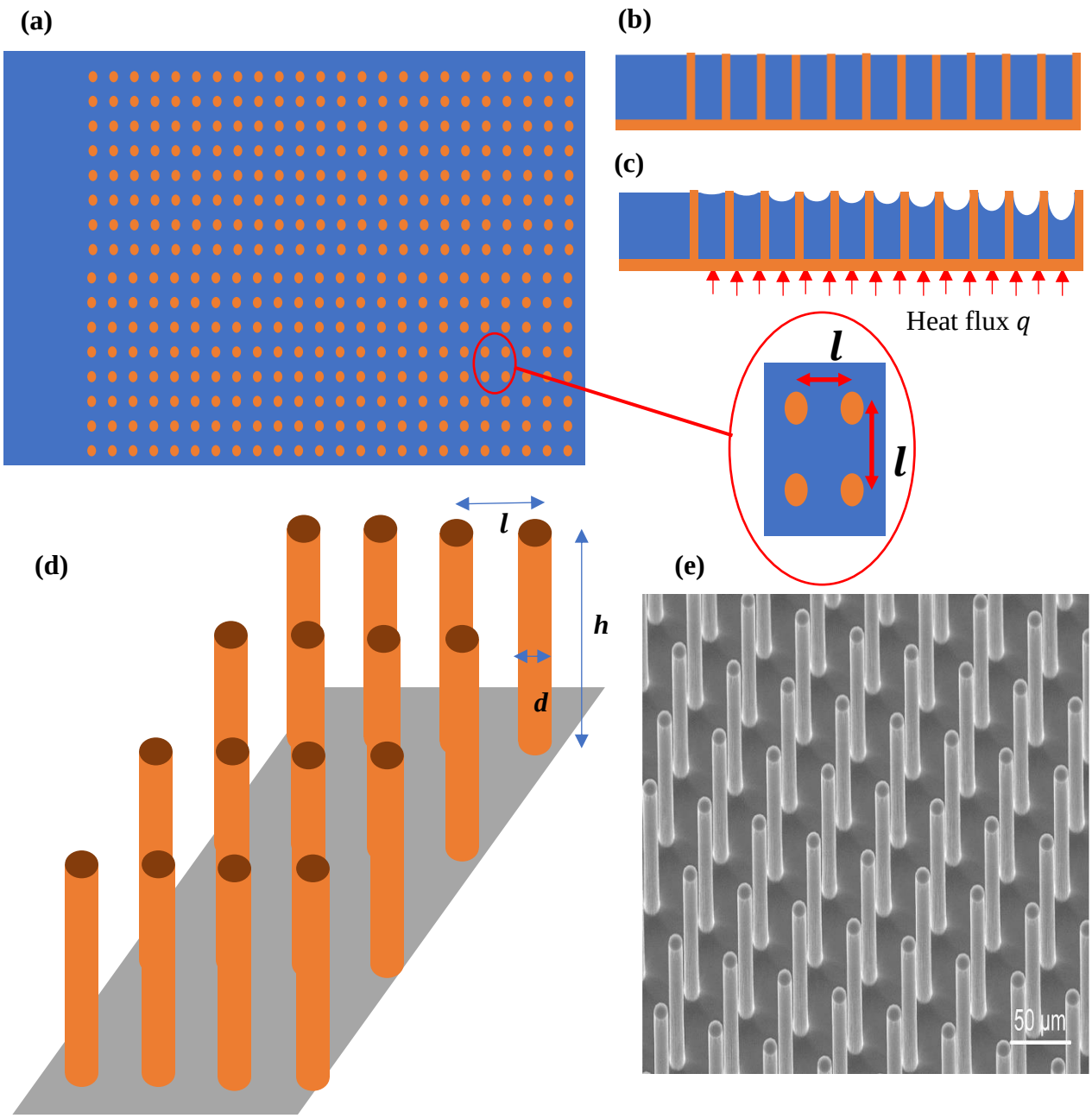

Figure 1. Thin-film evaporative cooler model: (a) top view of an array of micropillar wick structure with cylindrical geometry. (b) side view of the same geometry before applying heat flux (c) Side view of the structure when steady state condition is achieved after application of constant heat flux (d) a 3D view of the array. (e) Electron microscope image of a real constructed wick structure [8]

Figure 1 shows an example of a micropillar wick structure with a cylindrical shape. One side of the array is connected to the water reservoir, which has an infinite amount of water (theoretically). The water is filled inside the pillars due to capillary action. As the figure shows the distance between two consecutive cylinders in a row or column is uniform over the area and is defined as l. The height of the cylinder is defined as h and the diameter as d. Heat flux q is applied in the bottom surface.

Figure 1 (b) describes a situation where no heat flux is applied. When the heat flux is applied, the water starts to evaporate at a constant rate. The surface tension of the meniscus/ thin film formed around the pillars gives the pumping force to bring more water. The shape of this meniscus more specifically, the contact angle it makes with the pillars is very critical for our analysis. The shape of the meniscus is directly dependent on the pressure difference on both the side of the meniscus. The outer side vapor pressure is supposed to be the same for the whole cooling area. This is because the outer side is environmental air and should have ambient temperature and vapor pressure. The pressure on the inner side of the meniscus, which is water pressure changes with the distance from the reservoir. As the water flows due to the pressure difference and it passes through the flow resistance of created by the bottom surface, micropillars and the meniscus itself, so the pressure drops. The low pressure in the downstream increases the meniscus curvature. Figure 1 (c) represents this situation. The increment of curvature implies a decrease of the contact angle. It is known that for any liquid and solid pair, there is a minimum contact angle. This makes the limit to the distance water can be carried away by the wick structure or the end of the cooling zone. Once the minimum contact angle is achieved, the micropillars after that will not get any water supply because if the water pressure drops below that, the meniscus will not form. So, the grid will be left dry after that. This distance determines the effectivity of the wick structure. The more

pumping power means more wetting range, and that means more heat transfer rate; heat transfer is equal to the heat flux multiplied to the wet area. Figure 1(d) and 1(a) shows different characteristics dimensions: length between two consecutive micropillars in a row or column (defined as l), the height of the meniscus (defined as h) and the diameter of any micropillar (defined as d). Figure 1(e) shows an electron microscopic view of real silicon made micropillar structure [30].

Increasing the capillary suction force helps to increase the distance or in other words area of wetting. On the other hand, decreasing the pith and micropillar volume increases thermal resistance. So, there is a tradeoff between thermal resistance and capillary action increment.

2.4 MATRIX METAL COMPOSITE:

Matrix Metal Composite is a composite of two or more materials of which at least one is a metal, and others could be another metal, ceramic or an organic compound. It is done to get materials with improved properties of interest. It is a widely used technique in automobile, aerospace, biomedical, and many other industries [36] [37]. With the proper choice of materials, a matrix metal composite can provide higher thermal conductivity, lower coefficient of thermal expansion, higher elasticity, or toughness. Also, these materials are more wear and corrosion resistance and could be lightweight if the selection of the materials and the production method is chosen correctly. As a result, in almost every sector of engineering and manufacturing Matrix Metal Composite is replacing the traditional use of single material. For example, aluminum when used as reinforcing element with Boron, Carbon, Silicon Carbide or graphite for composite making, the product could be 30% to 40% stronger and more rigid compared to the use of only aluminum [36]. It is predicted that the worldwide market of metal matrix composites will reach 10.8 kilotons per by the year 2021 [36].

A matrix metal composite has three distinct parts: the matrix, the reinforcement, and the interface between reinforcement and the matrix. The matrix is the structure made of the continuous phase of composites and used to hold the reinforcement in the desired shape, size, and orientation [37]. Reinforcement is a stronger material than the matrix element and is distributed inside the matrix to give more advanced properties. These matrices and the reinforcement can get mechanically locked or can be bonded chemically. Three of these elements' matrix, metal, and the interface are necessary to determine the properties of the compounded product. Any error or inability in the production process can change any of these elements and thus can result in a product of undesirable property values even though the constructing materials are the same.

There are many options for the materials of composite and the reinforcement as well. They are chosen based on desired properties of the product, interaction of the materials, manufacturing process, and cost of production. Among them, the use of Titanium, yttrium, zirconium, and hafnium as reinforcement material is very remarkable as they serve many desirable properties with a cheap production method. Titanium matrix composites (TMCs) serves high specific strength and stiffness in contrast to the composites made from steel and nickel-base materials. It can also provide a 50% weight reduction in comparison with monolithic superalloys while offering the same stiffness [38]. Studies also show the effect of yttrium in increasing hardness of the composite [39]. Zirconium and some zirconium compound have shown the excellent quality of refractoriness, high resistance to abrasion and thermal shock and also chemical attack when used in metal matrix composite [40]. Also, hafnium has uses in metal matrix composite formation.

One of the popular methods of manufacturing these metal matrix compounds is to make the liquid metal (reinforcement one) to flow through the porous matrix made by another metal or ceramic or any other material. Understanding this flow physics is very important because due to an error on this stage of production, the inner core of the matrix could be left unfilled or filled with unwanted materials (e.g., air bubble). It is impossible to observe or study this flow pattern physically due to the concealed matrix and high-temperature metal. Hence, a 3d modeling of this flow of the molten metal through this porous matrix is needed to be developed to study its characteristics.

2.5 EXASCALE PORE NETWORK SIMULATOR:

The EXPNS algorithm is developed to solve the porous flow physics both in pore scale and network scale. Previously, two-phase flow in porous media has been studied from multiple perspectives to include the findings in experimental observation, theoretical formulation, and computational modeling [41]. To discover this porous flow physics studies has been done from both experimental and numerical approach [42] [43] [44]. Among them, many was based on network modeling type [45] [46] [47] [48] [49].

The flow-through porous media could be two types; miscible or immiscible. In the case of miscible fluids, there are no separating interfaces inside the flow zone. However, in the case of miscible fluids, there are separating interface between two flow. Moreover, also the viscosity and associated resistance will be different for two separate portions. The total resistance, in this case, is the sum of the resistance generated by each fluid. The miscible flow can be designed as a flow of single-phase fluid, but the former cannot be. For example, oil and water do not get mixed and maintain a distinct boundary between each other. So porous media flow with two or more fluids separated by distinct interfaces are referred to as multiphase flow systems. Our EXPNS is focused on two-phase flow system.

Predicting a future state when initial and boundary conditions are provided is needed to exploit a system. Depending on the application criteria, a decision must be made up to how details the prediction is needed and so how the model will be designed. A porous media can be viewed in four different length scales [50]. The first is the most details; is discernible only through scanning electron microscopy or thin sections. This is called pore or microscopic scale. The Navier-stokes formulation at this scale usually can predict the fluid flow. Sometimes in this level, due to increased complexity by multiple interfaces among multiple fluids inside the complex solid matrix, it poses

an immense computational challenge, and it becomes impossible to solve the flow physics. The next scale is the core or macroscopic scale. A core of pours rock is taken from the source, and empirical correlations are developed from laboratory data by proceeding some standard tests. Next comes the megascopic scale where the entire reservoir is modeled considering it as a collection of millions of cores. The final level is the Giga-scopic scale where an entire area is considered consists of varieties of a reservoir.

The EXPNS works one step up from the pore-scale but not the same as the core scale. It stands in between core and pore scale. The flow in every pore is not calculated in detail, but the mass balance is maintained accurately at the pore level. With that, an assembly of pores is modeled, and the flow of that network is observed and analyzed. The flow details at pore levels are avoided here as that approach require extensive computation challenge; cannot be handled by the supercomputers of modern time. Many commercial packages have attempted to do so but considering the details pore level flow and considering an assembly of billions of pore at the same time seems to be impossible due to extensive computation power required [51] [52]. So, in this work, the EXPNS is modeled in such a way to avoid tiny details in pore level. However, the journal of mass balance is maintained at the pore level. With those calculations from the pore level, an assembly of pores is made to elevate it to a network level. Each pore here is modeled as a cylindrical pipe with an initialized radius and length (The details of these modeling is discussed below) On contrary to the lab tests of cores where the inside structure is not taken into consideration, here the EXPNS considers the exact distribution of the length and radius of the actual pores. The pores defining parameters are selected in a way so that they follow some preselected distribution. These distributions can be known from microscopic observation of the thin physical section of a porous matrix.

CHAPTER 3: PROBLEM DESCRIPTION

In this thesis, two problems are simulated by the EXPNS, and the flow pattern was analyzed. One is the analysis of the flow of water through a micropillar cooling system with an applied variance of two of the geometrical parameters (radius and length). Another one is liquid metal flow through the matrix of a Metal Matrix Composite. The goal of these simulations and the challenge of the modeling are described below:

Problem 1: Flow-Through Micro Pillared Cooling System Analysis:

A brief description of the working principle of micro pillared wick structured cooling system is given in section 2.3. Much rigorous research has been done and proved the cylindrical geometry as the optimum geometry for the wick structure [53] [54]. Also, studies have been done to find out the optimal geometrical parameters of the chosen geometry [55]. However, an underlying assumption on all these studies was that all the geometrical parameters such as height and radius of the cylinder pillars and the distances between each row and column are the same throughout the device. Which is correct but only in a hypothetical situation. However, in reality, it is pervasive to have a variance of these parameters due to manufacturing inaccuracy. Also, this variance can be made voluntary to achieve far more effectiveness, which is kept unexplored because of not being able to simulate a full-scale scenario. All the previous studies mainly analyzed the flow through a unit cell and then predicted the entire case scenario based on that. While they kept in consideration that all the cylinders have the same geometrical parameter and arrangement throughout the surface they stand upon. This was done mainly to avoid the complexity of the numerical simulation arrives when this variation is counted. As the parameters vary the resistance of flow through the unit cell varies accordingly. This led to a non-uniform pressure distribution of two adjacent cells in a row.

This introduces cross flow over the geometry, and which multiply the complexity of the simulation. An example of the case has been imaged in figure 2.

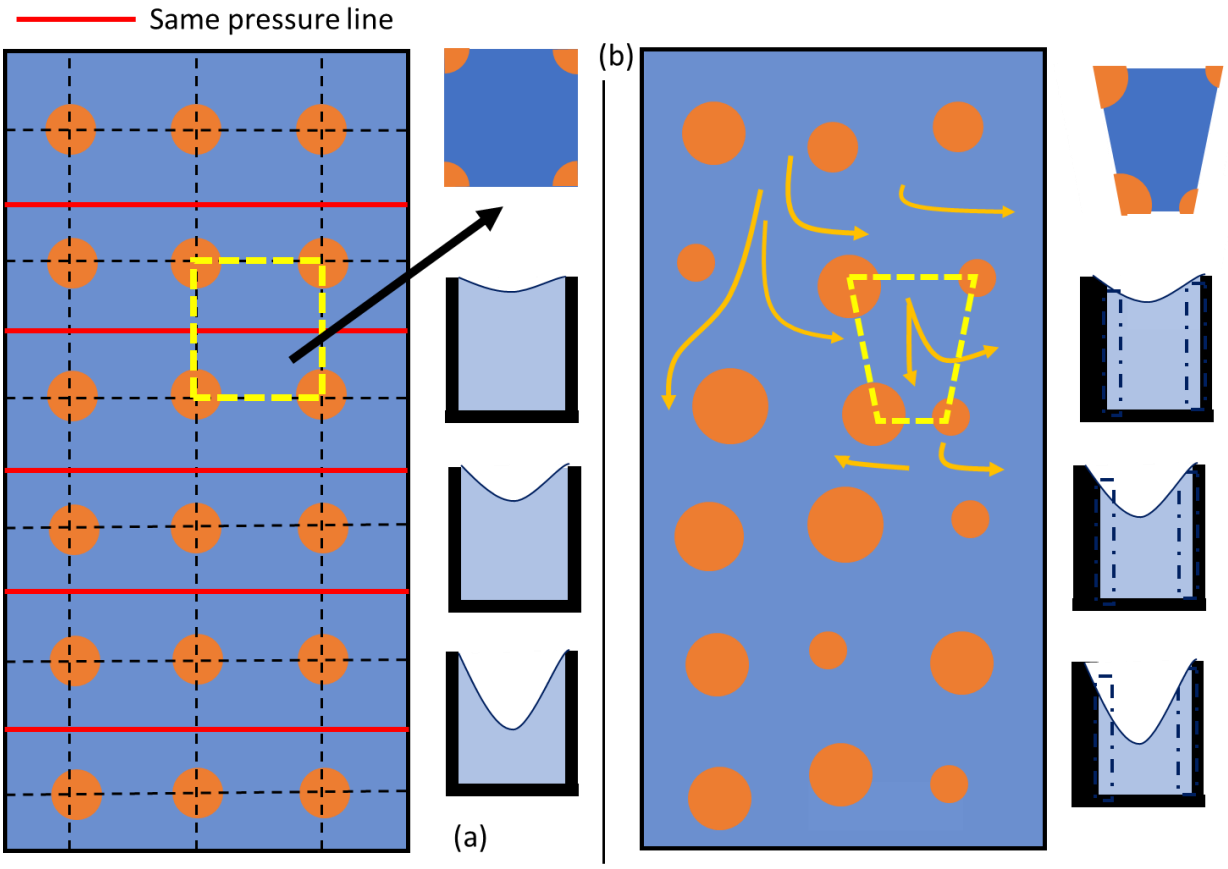

Figure 2: (a) Each parameter is same for all the cylindrical pillar. (b) Variance in parameters over the region and resultant cross flow. The yellow dotted boxes represent one single cell for analysis. The side figures show different contact angle situation of the boxed cell

For the described case of the figure2, the pressure in any two adjacent cells in a row is always equal due to the symmetric condition. The edge columns are different, but, in the calculation, the symmetric boundary condition is applied. In reality, they do not affect much due to a vast number of pillars in the square. In work [55], they have done rigorous work to find out the optimum ratio

of radius, height, and distance between two cylinders. For optimum case, it was found that $\frac{d}{h}$ is approximately equal to 0.4 and l/d is approximately equal to 3.

The shape of a meniscus in a single cell is determined by the force balance equation named young Laplace. According to the Young−Laplace equation $P_{vaper} - P_{liquide} = 2\sigma k(x)$, where σ is surface tension force, and $k(x)$ is the curvature of the meniscus. In our case, we can write $\left(P_{vaper} - P_{liquide}\right) * (l^2 - \pi r^2) = 2\pi r\sigma \cos\theta$. While θ is the average contact angle [55]. Here, P_{vaper} is the ambient air pressure and $P_{liquide}$ is the pressure produced by the liquid at the bottom of the meniscus. As the device is kept in a room pressure which is one barometric pressure and the air around is considered to be 100% saturated (for calculation convenience), so with the advancement of the flow, the pressure of the fluid will drop gradually as the water will pass through resistances. So, the contact angle will decrease while increasing the curvature of the meniscus to support the pressure difference from both sides (air and water). This is explained in figure 1(c).

Now having variability in diameter and distance between two rows/ column may contribute to more effectiveness. The effect of height, h is straight forward. Increasing h reduces the resistance, but it does not have any adverse effect on the meniscus of flow unless the height is too low. So, the effect of the height is not considered in this study. For the height, we can follow the instructions from the previous studies like [55] [56]. In this work, we only focused on the effect of the diameter variation while keeping the pitch, l ,and height fixed. Studies of other kind of variation is a scope for future work.

If in a single cell the radius of the four cylinders is kept equal (like figure 2(a)), changing the radius (all together) will change the effect on the flow. With the increment of the diameter, d the flow resistance increases as the volume to pass become narrow. Which increases the pressure gradient

of the cell and so lower pressure on the next cell results lower contact angle. This means the meniscus is more curved, which results to decrease the flow area and so more resistance (increasing the boundary layer resistance) [57] [58]. However, this increases the contact line for the meniscus on that single cell. So, the meniscus of that specific cell becomes less curved as it can produce the same force on a higher angle. This way, the boundary layer resistance of that meniscus decreases. Also, due to the area shrinkage (if seen from the top) reduce the force on the meniscus as force is the area multiplied with the pressure upon it. Which also help to decrease the curvature. Figure 3 shows an example of this scenario. So, increasing the diameter, d will not necessarily increase the flow resistance. Instead, it is a complex calculation including the flow analysis through the cell and the force balance equation for the meniscus. The flow is driven by the meniscus force, so creating more contact line will add up more force to the flow while increasing the diameter will slow down the flow by imposing more flow resistance. However, this trade-off between meniscus curvature and flow resistance indicates strategically setting up of variable diameter over the region may benefit us more with additional heat transfer capability. Besides the cylinders could have a variable diameter due to manufacturing inaccuracy. So, doing a simulation of equal diameter will not unveil the real-life scenario.

Now if four of the cylinders have different diameters and there is no fixed pattern throughout the array, it will be a very computation intensive work to find out the flow. However, this analysis can help us to understand the flow physics more accurately. Also, it may open a path for adding the extra capability of heat transferring.

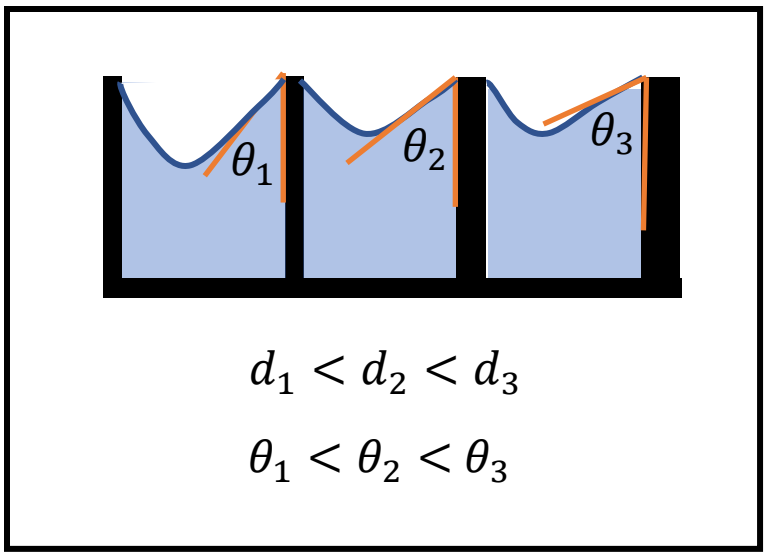

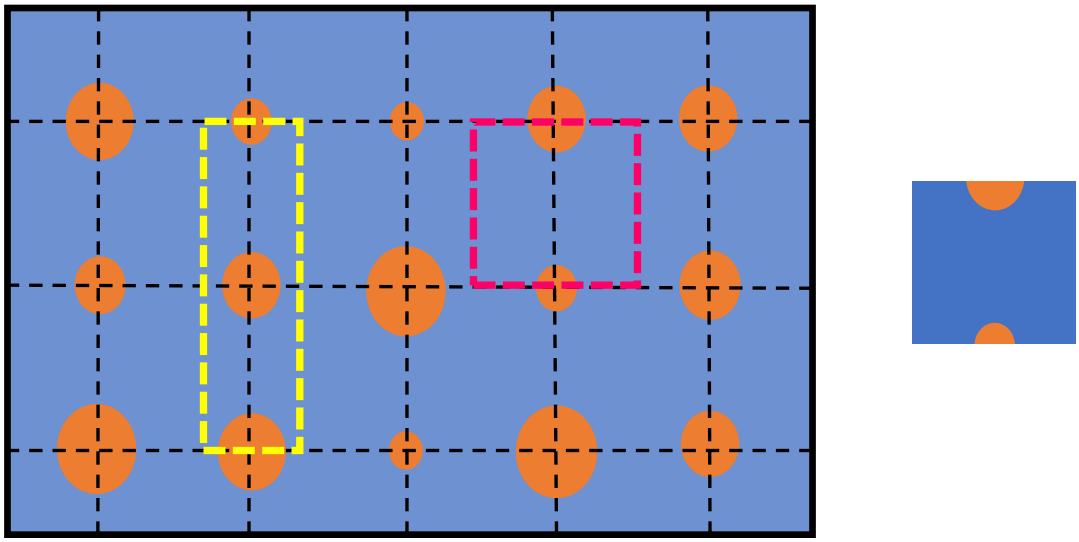

Figure 3: An example of change of contact angle with the change of diameter

To do the full-scale simulation of these variable cylindrical structures, it is essential to find out the flow resistance of these structures. The EXPNS working principle is described in the methodology. For finding the resistances for full-scale simulation cells like figure 3 is considered (the pink one). There will be numerous different cell architecture based on the diameters. For each of these cases also there will be subcases as we must consider different heights. The highest height will be when

the contact angle tends to zero, and the lowest height will be when the contact angle is minimum. Why cells are considered in this shape and how many architectures we will have is widely described in the methodology section.

In this thesis, we approached to find out the resistance of these cells with a variable combination of diameters. Applying these data for a full-scale simulation is kept for the future extension of this work. For full-scale simulation, we will use the modified EXPNS, and these data sets to predict the real case scenario.

Problem 2: The Flow Of Liquid Metal Through Matrix Metal Composite:

For producing a matrix metal composite, a reinforcement material is dispersed into a matrix which usually a lighter material. One of the widely used methods of forming a matrix metal composite is to infiltrate the liquid molten metal into a porous matrix (usually ceramic) [38]. The nature of this flow is very different from organic flow due to high interfacial energies of liquid metal [39] [40]. As the flow through the porous media is driven by the surface tension force and the pressure force applied the flow rate is much dependent on this surface energy [41]. Numerous experimental studies of molten metal flow through porous matrix have been done. One of the critical parameters for flow advancement is the contact angle. In the case of $\theta<90°$, we may get a better infiltration where, on the other hand, $\theta>90°$ may leave void areas in the matrix [42]. However, when $\theta<90°$ it may degrade the matrix material due to reactive wetting angle. With $\theta>90°$, there is not matrix degradation, but infiltration is not good [42]. Also, it was observed that a large volume fraction is left unoccupied by the invading molten metal (Cu, Zn, Al) due to this wettability in a silica gel made matrix [43]. Some other studies like [44] describe the flow of silicate glasses at 1200 degree Celsius over molybdenum. Also, the spreading of molten Cu, Au, and Ag over Mo is studied here [45]. The velocity of molten aluminum alloys at 670 degree Celsius is discussed in the paper [46].

Many Numerical modeling to explore the science of metal flow is also done [47]. To find out the depth penetration and flow velocity, a numerical study had been done for a single capillary tube [48]. Also, some other numerical studies describe the effect of centrifugal force to facilitate the flow through the media [49]. However, that also consider only a single pore. In contrast, in the paper [50], a stochastic model is considered for pore distribution to predict the uncertainty of the flow of invading liquid.

Though there are many studies done already on metal flow through porous media, none of them considered the flow phenomenon in a massive scale. In this thesis, the flow is observed by using a numerical model of Exascale pore network simulator (EXPNS) developed by my research group [51]. Our purpose is to observe the pressure distribution with time and penetration rate of the first fluid. The simulator was developed in an object-oriented fashion. Next-generation computing platform like Trilinos and Kokos (developed in Sandia national Lab, USA) have been used in this algorithm. The simulator is applicable for massively parallel architectures and scalable up to 50 million in general. This massive scale will help us to understand the flow physics in large scale more accurately than interpolating the results of one pore to many pores. The mechanism of the EXPNS is described in the methodology section.

CHAPTER 4: METHODOLOGY

4.1 THE NETWORK-RESISTANCE MODEL TECHNIQUE FOR A POROUS MEDIA FLOW AND THE WORKING PRINCIPLE OF EXPNS:

A porous flow includes one or more viscous fluid flowing through a porous elastic or inelastic structure [59] [60]. This porous structure is formed by a combination of void and solid fractions. The fluid passes through the void area. The geometry of this void or solid part is very irregular, except the matrix is created by any advanced manufacturing technique. This void geometry can be modeled as a stochastic distribution [61]. However, that approach invites enormous complexity with it.

In EXPNS, we only focus on elastic porous media and the pores are simplified as cylindrical pipes, but to keep the randomness of the original structures, the radius and heights are distributed following any given distribution. This way, the complexity of modeling a complex irregular shaped geometry is avoided, but the effect of this irregularity on the flow is reserved very accurately.

A description of the above literature about porous flow can be seen in figure 2 [62], 3 [63], and 4 [64] on the next pages.

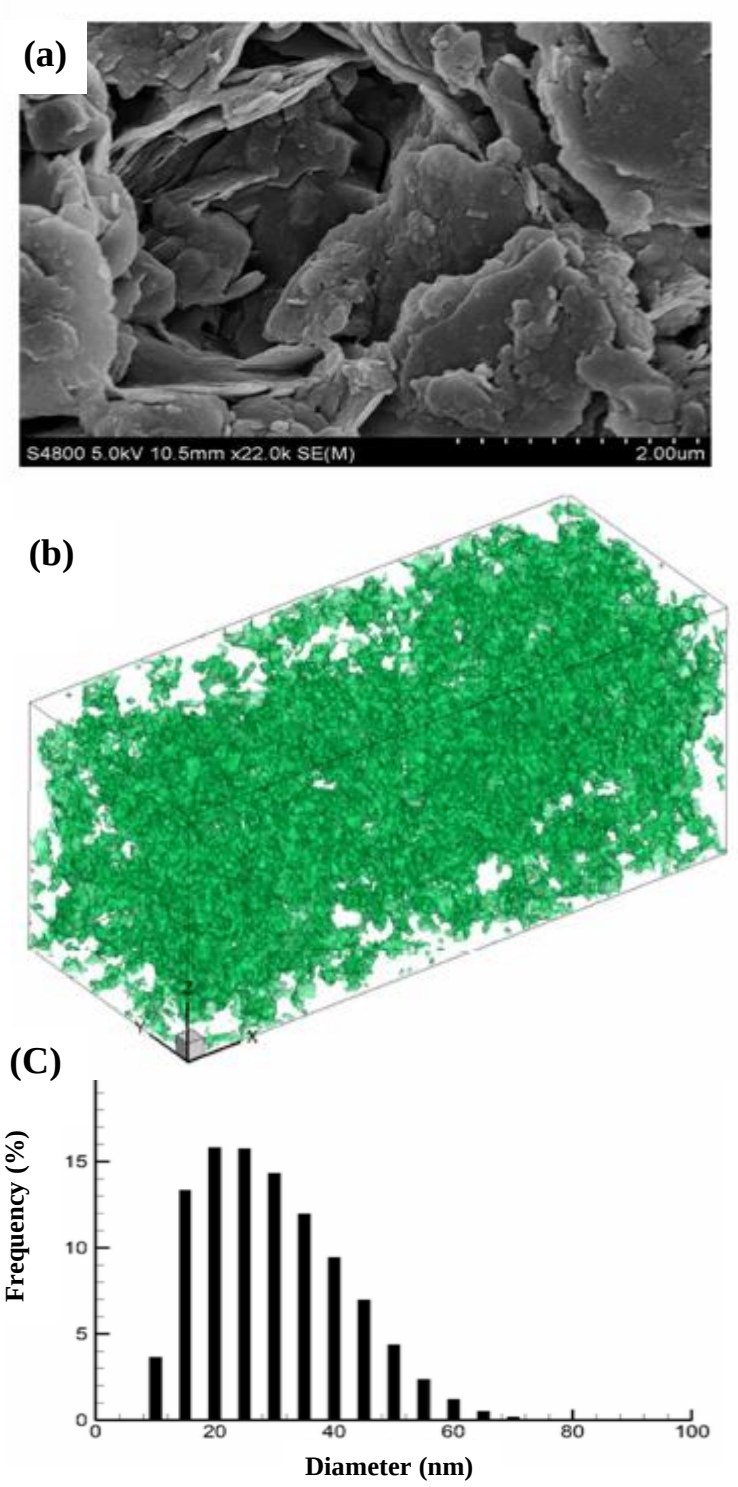

Figure 4 [66] Nature of pores: (a) A scanning Electron Microscopic image of a shale samples from Sichuan Basin China rock (b) 3D reconstructed porous structures of shales (c) pore size distribution of the reconstructed shale

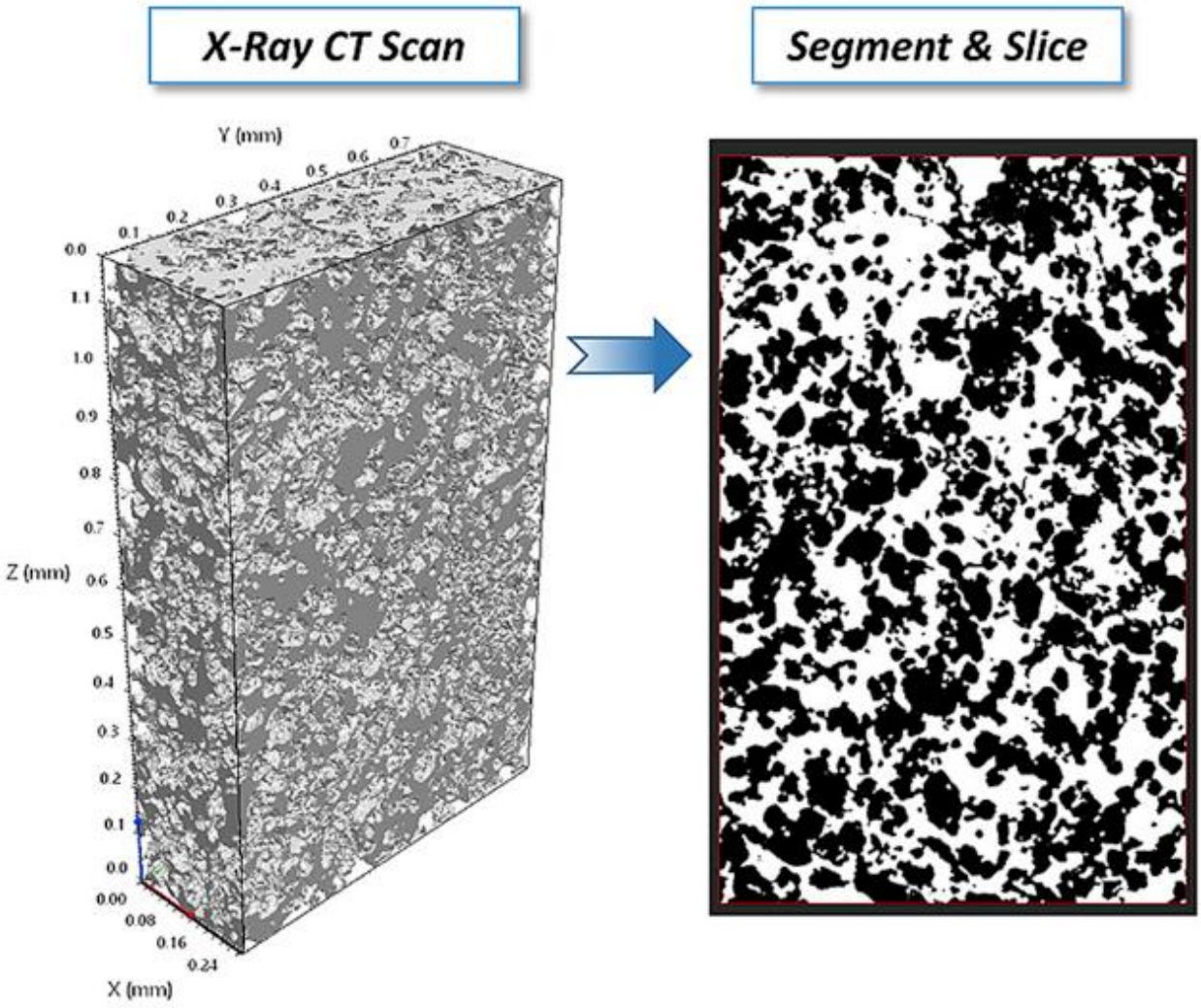

Figure 5 [67] Model of a porous medium: *(a) 3D rendering of a porous media generated from CAT scanning (b) Segmented 2D cross section of a porous medium. Black shapes are air and white shapes are ceramic. The picture was obtained with the help of a technology called X-ray computed tomography imaging*

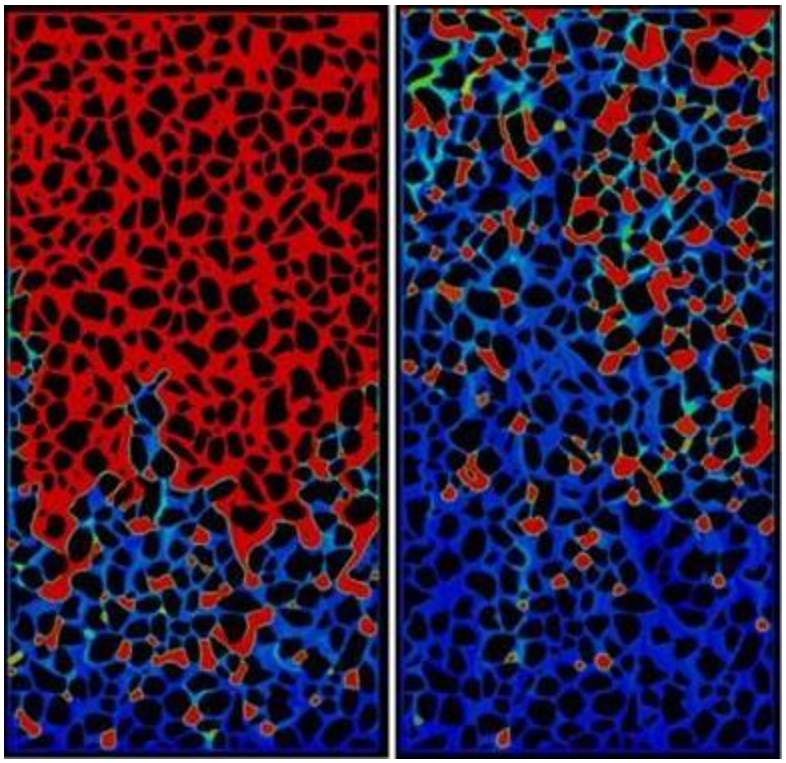

Figure 6: An example scenario of fluid two fluid flow through a porous media 2D section. Red and blue indicates two different fluid and the black is the matrix material

The above image shows how, in reality, how the fluid flows through a porous media. In a porous medium which is collected from the environment or made in such a way that the geometry of the matrix is very irregular, trapping of the defending fluid is widespread. Though the amount of the trapped material varies a lot based on the matrix and the two-fluid interacting. Usually, this trapped fluid amount is very less compared to the void volume of the matrix. There have been several studies shows determining the trapped amount and the technique to recover them [65] [64] [66] [67] [68] [69] [70] [71] [72]. A study [73] also shows how wettability effects efficiency of the invading fluid on removing the defending fluid and thus make less trapped fluid zone. Also, it describes techniques to change the wettability of fluid for getting optimum removal of the

defending fluid. However, for most of the cases, it has been observed that when the wettability is chosen wisely for the advancing fluid most of the defending fluid can be removed and only a very little can be get trapped [68] [70] [73] [74]. In these studies, it is observed that besides the properties of the two fluids, the structure is also a parameter contributing to the trapping of the fluids.

In this work, we have not taken consideration of this defending fluid getting trapped explicitly. However, the modeling does take consideration of this phenomenon implicitly. As mentioned before that the pores are modeled as pipes in EXPNS network-based modeling system when the pipe radius is small, and the length is bigger it acts similarly to the geometry of complex irregular pore which traps the defending fluid. As because of smaller radius and bigger length, it poses higher resistance to fluid flow and so it will be harder or impossible for the invading fluid to capture that area. Also, the EXPNS works on counting the invading fluids volume fraction. It is considered that if in any node the invading fluid is reached then any output from that node will be by the invading fluid.

It was mentioned before, that for modeling the pore medium while avoiding the complexity, each pore is considered or modeled as a pipe while the radius and length of these pipes are assigned at the beginning in a way so that they flow any given distribution. For clarification here is a picture of the model we are describing (Figure: 5)

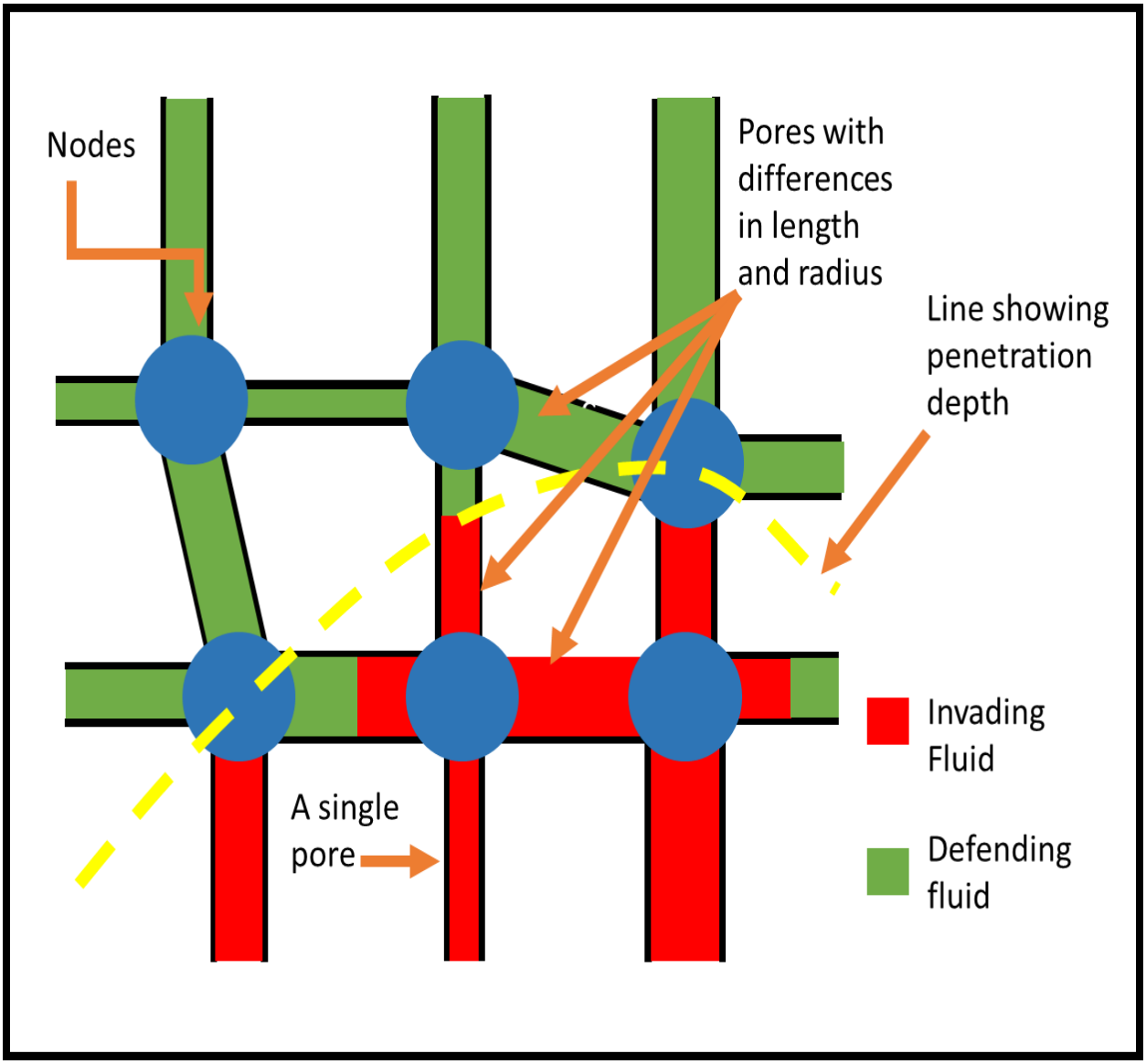

Figure 7: Shows connections of pores. The variation of radius and length can be seen from the figure. The blue circles are the nodes. Each node is a junction point of four pours. The Yellow line shows penetration depth varying with X axis

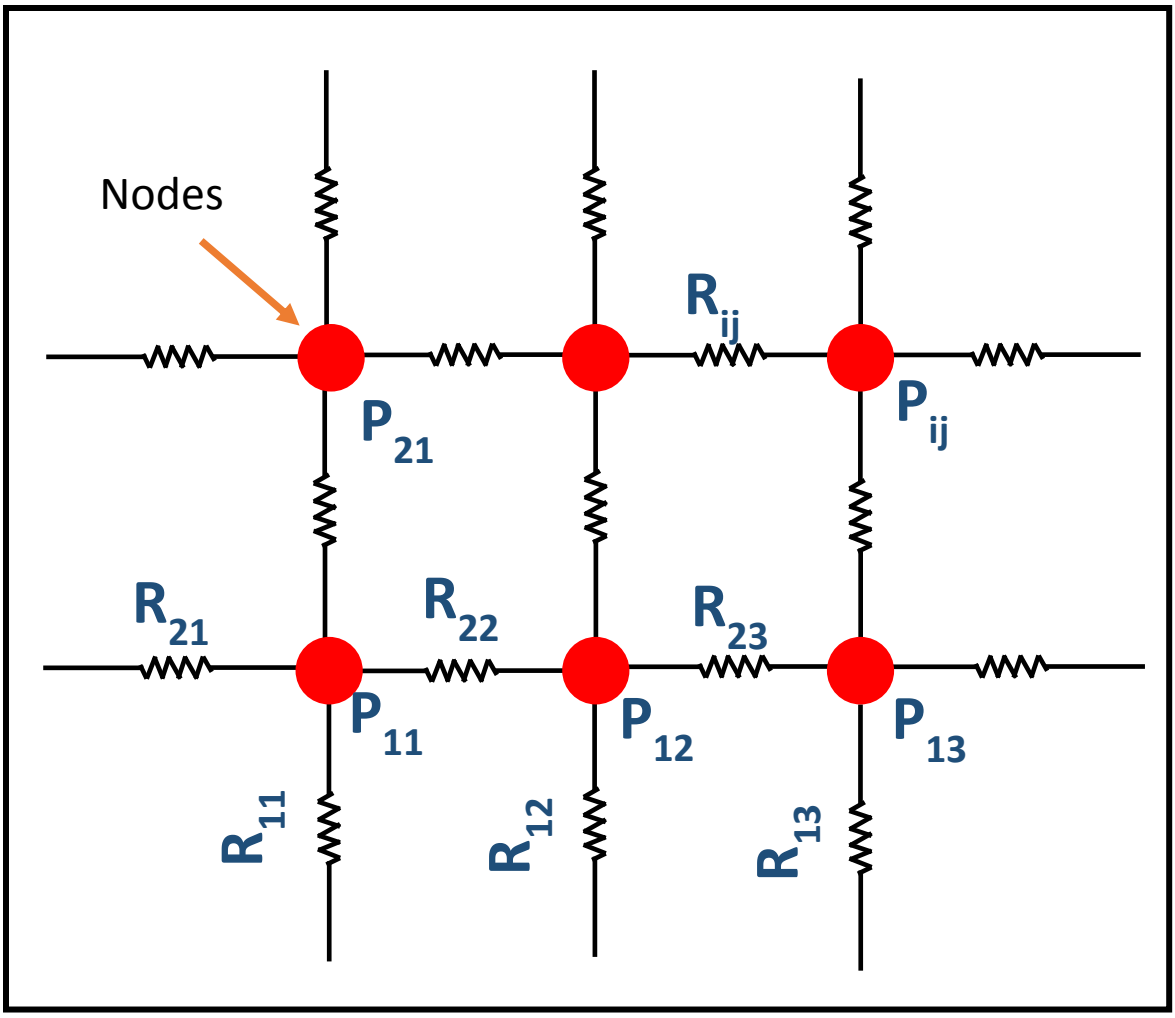

Figure 8: Shows the network representation of the figure 5

Here in figure 6, the network modeling representation of figure 5 is shown. The pipes are replaced with the calculated resistance from radius, length, and depth of penetration. This depth of penetrations involvement in flow resistance will be described in the following article. Moreover, the pressure of nodes is found out by one-step run of the algorithm. Thus, a pore medium becomes a network of connections between nodes with different resistances.

For more network modeling in EXPNS, each pore is considered as a pipe of radius r and length l, and they are connected in nodes with others. EXPNS can simulate only 2D porous flow. Each pipe in the network is initialized with a length and radius following a given distribution. For simulating a real-life material, the distribution is chosen from the microscopic structure of the material.

The flow inside a pipe can be simulated by using Navier-Stokes formulation. Which is:

$$\frac{\partial}{\partial t}(\rho u_t) + \frac{\partial}{\partial x_J}(u_i u_J) = \frac{\partial}{\partial x_J}(\frac{\mu \partial u_J}{\partial x_J}) - \frac{\partial \rho}{\partial x_i} \qquad \textit{Eqn:10}$$

Considering the flow incompressible, laminar and axisymmetric [75], we get:

$$\frac{\mu \partial^2 u}{\partial r^2} = \frac{-\partial p}{\partial x} \qquad \textit{Eqn:11}$$

This equation can be solved assuming linear pressure difference in to:

$$Q = \frac{\Delta p\, \pi r^4}{8 \mu x} \qquad \textit{Eqn:12}$$

Where x indicates the length of the pipe occupied by the fluid, r indicates pipe radius, μ is fluid viscosity, Q is the flow rate, and Δp is pressure difference. It is a linear relationship between pressure difference and flow where others term can be considered as conductance $k = \frac{\pi r^4}{8 \mu x}$. As in this case, it is considered that another fluid already exists inside, and the invading fluid have to remove it from the porous medium the effective conductance changes into $k = \frac{\pi r^4}{8(\mu_1 X_1 + \mu_2 (l - X_1))}$. Where μ_1 and μ_2 are the invading and defending fluid's viscosities and X_1, $(l - X_1)$ are the length

of invading and defending viscosity respectively. The following figure describes the difference in single fluid flow and multi-fluid flow:

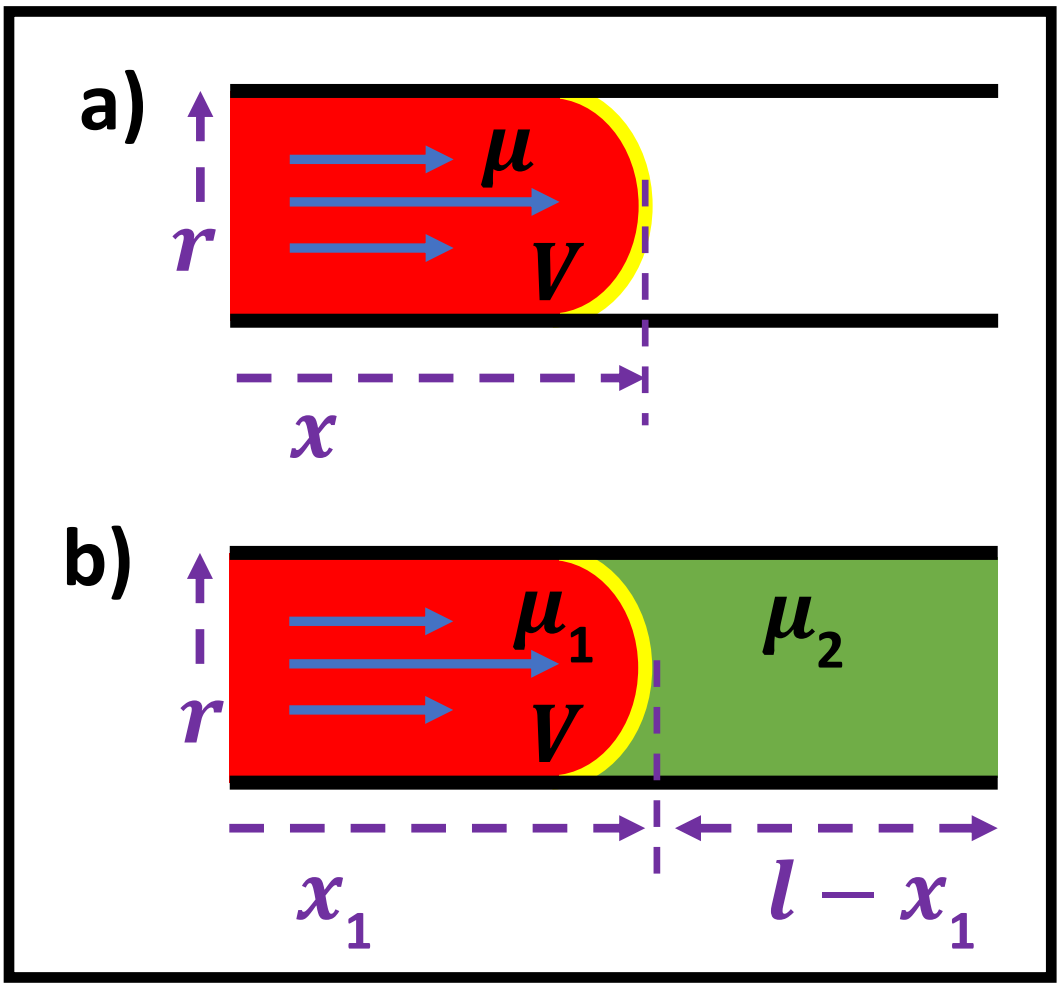

Figure 9: (a) Flow of a single fluid. (b) Flow of two fluids

The figure above shows when it is only one fluid the resistance due to viscosity is only due to the invading fluid itself, and so the length is only the penetrated length. In contrary, for two-fluid flow condition: as the invading new fluid must remove not only itself but also the defending fluid, so the resistance is the sum of the resistance created by both the zone. So, in that case, the length in the equation is both X_1 and $l - X_1$.

It can be understood from the equation (12) that with the advancement of the invading fluid, the conductance will be changed and must be calculated in each time steps; until the pipe is filled with one single fluid. The problem has been designed as a marching problem where each time steps the pressure distribution is calculated assuming a quasi-static behavior of the fluid. From which the flow and the volume fraction is calculated. With a new volume fraction, the conductance needed to be re-calculated.

For keeping the journal of conductance mentioned above in between any two consecutive steps of pressure measuring, EXPNS uses a Directed acyclic graph; nodes are considered as vertices and edges are the conductance. As per the previous discussion, we can write the flow rate between any two nodes at time t as:

$$Q_{i,j} = \left(P_i - P_j\right) * \frac{\pi {r_{i,j}}^4}{8(\mu_1 Y_{i,j}^t + \mu_2(l_{i,j} - Y_{i,j}^t))} \qquad \textit{Eqn:13}$$

$$\gg \frac{dY_{i,j}}{dt} = \left(P_i - P_j\right) * \frac{{r_{i,j}}^2}{8(\mu_1 Y_{i,j}^t + \mu_2(l_{i,j} - Y_{i,j}^t))} \qquad \textit{Eqn:14}$$

$$\gg Y_{i,j}^{t+dt} = Y_{i,j}^t + \left(P_i - P_j\right) * \frac{{r_{i,j}}^2}{8\left(\mu_1 Y_{i,j}^t + \mu_2\left(l_{i,j} - Y_{i,j}^t\right)\right)} * dt \qquad \textit{Eqn:15}$$

And so, the conductance becomes:

$$k = \frac{\pi r^4}{8(\mu_1 X_1 + \mu_2(l - X_1))} \qquad \textit{Eqn:16}$$

An example of DAG for a 3*3 pore network is shown below:

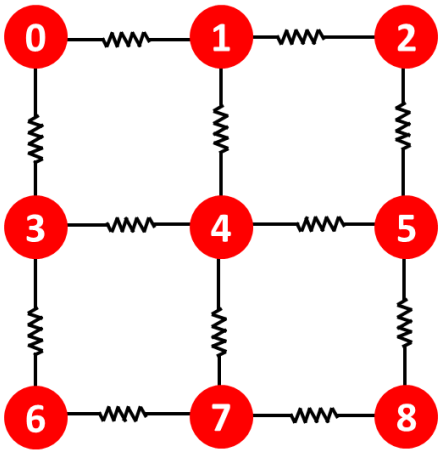

	0	1	2	3	4	5	6	7	8
0		K_{01}		K_{03}					
1	K_{10}		K_{12}		K_{14}				
2		K_{21}				K_{25}			
3	K_{30}				K_{34}		K_{36}		
4		K_{41}		K_{43}		K_{45}		K_{47}	
5			K_{52}		K_{54}				K_{58}
6				K_{63}				K_{67}	
7					K_{74}		K_{76}		K_{78}
8						K_{85}		K_{87}	

Figure10: An Adjacency matrix of the conductance for a 3x3 pore-network model

Now for any single node, the calculation is described below:

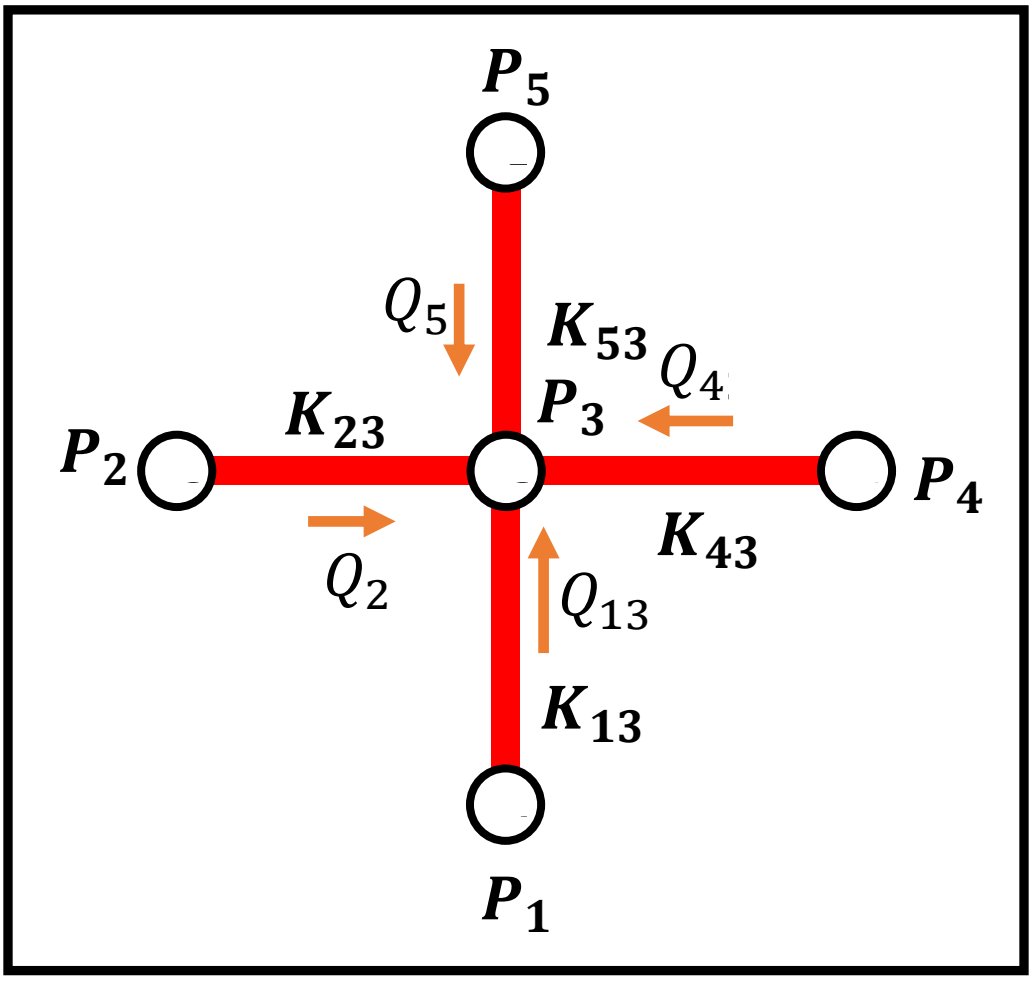

Figure 11: Figure explaining flow into a single node

From figure 7, we can write:

$$Q_1 + Q_2 + Q_3 + Q_4 = zero/constant \qquad Eqn:17$$

As nodes do not store any fluid, and the flow is incompressible, the sum of all the flow towards a node should be equal to zero. However, if the fluid is getting out at a constant rate (e.g., due to

evaporation or leak), then it will be a constant value. Example of this situation is our second project.

In this case, the flow happens due to the pressure difference created by the external pressure difference (given as a boundary condition) and the capillary pressure. The capillary pressure could be calculated by the equation:

$$capilary\ pressure, P_c = \frac{2\pi r\sigma \cos\theta}{\pi r^2} = \frac{2\sigma \cos\theta}{r} \qquad \textit{Eqn:18}$$

The wetting angle θ is fixed for two specific liquid and the matrix material. Now, as described earlier equation 12 becomes:

$$Q = (\Delta p + P_c) * \frac{\pi r^4}{8(\mu_1 X_1 + \mu_2 (l - X_1))} \qquad \textit{Eqn:19}$$

alternatively,

$$Q = (\Delta p + P_c) * K \qquad \textit{Eqn:20}$$

Were, $K = \frac{\pi r^4}{8(\mu_1 X_1 + \mu_2 (l - X_1))}$

From this we can rewrite the equation 13:

$$(P_1 - P_3 + P_c) * K_{13} + (P_2 - P_3 + P_c) * K_{23} + (P_4 - P_3 + P_c) * K_{43} + (P_5 - P_3 + P_c) * K_{53} = zero \qquad \textit{Eqn:21}$$

Which can be rearranged to:

$$P_1 * K_{13} + P_2 * K_{23} + P_3(-K_{13} - K_{23} - K_{43} - K_{53}) + P_4 * K_{43} + P_5 * K_{53} + P_c(K_{13} + K_{23} + K_{43} + K_{53}) = zero \qquad \textit{Eqn:22}$$

Now for all the nodes, we will have an equation like this, and all of them can be arranged in a format like $AX = b$.

Modified Nodal analysis is applied to find the pressure distribution and the flow rate by solving one single $AX = b$ equation.

Once the flow rate is known, applying the modified Euler method, the advancement of the invading fluid in each pipe/connection is measured. By this way, the fraction of two fluid is changed inside a pipe. From that using the formula for the conductance new adjacency matrix is derived. Now the system is ready for calculating next steps displacement using this newly formed adjacency matrix. Thus, this cycle repeats until it exceeds the given time limit.

4.2 VALIDATION OF EXPNS:

For Validation of EXPNS, it is compared with the capillary flow through a capillary tube predicted by Rhine's Equation [76]. Rhine's equation gives a transient solution to the capillary rising through a capillary duct. The work [76] modified the Rhine's equation and included the consideration of inertia force. The equation becomes:

$$\frac{d}{dt}\left(\pi r^2 h \frac{dh}{dt}\right) = 2\pi r\sigma\cos\theta - 8\pi\mu h\frac{dh}{dt} \qquad \textit{Eqn:23}$$

Here, h is the depth of penetration, and θ is the contact angle.

This equation has a solution like this:

$$\frac{dh}{dt} = \frac{\Delta p\,\pi r^4}{8\mu A h} \qquad \textit{Eqn:24}$$

Here, Δp is the pressure difference between two nodes and supposed to be equal to

$$\Delta p = (P_i - P_j + P_c)$$

However, in Rhine's equation, it is considered There is no external pressure so $P_i = P_j$ so $\Delta p = P_c$

Where,

$$capilary\ pressure, P_c = \frac{2\pi r\sigma\cos\theta}{\pi r^2} = \frac{2\sigma\cos\theta}{r}$$

It can be written as (For two-fluid):

$$h_{t+dt} = h_t + \Delta p * \frac{r^2}{8(\mu_1 h_t + \mu_2(l - h_t))} * dt \qquad \textit{Eqn:25}$$

In order to simulate a single-phase flow μ_2 is considered approximately zero. Moreover, to avoid truncation error, a modified Euler method was used:

$$(h_{t+dt})^2 = (h_t)^2 + \Delta p * \frac{{r_{i,j}}^2 * h_t}{8(\mu_1 h_t + \mu_2(l - h_t))} * dt \qquad \textit{Eqn:26}$$

With these conditions, a 3*1 pore network was simulated and verified with the result from the Rhine's Equation. Some comparisons of different flow parameters between Rhine's equation and EXPNS single-phase flow in a 3*1 matrix is shown in the result section.

4.3 **LIQUID METAL FLOW**

For the liquid metal flow analysis, we simulated four liquid metals: Titanium, Hafnium, Zirconium, and Yttrium. The reason behind choosing these materials is their usefulness for constructing matrix metal composite (Details can be found in section 2.4). The sole purpose of this work is to observe the pattern of these liquid metal flow when simulated in EXPNS.

For simulating the single-phase flow of these molten metals inside the matrix we considered the defending fluids viscosity and surface tension approximately zero. This was needed to be done because the EXPNS was basically designed for two-phase flow.

For the invading liquid metal, we gave input its property values such as surface tension, viscosity, and the contact angle. These parameters define a fluid when flow through a porous media (excluding the effect of gravity as we consider horizontal flow). The values of these physical properties were considered for two temperature; one at the metals melting point and another at 2300 degree Celsius which higher than any of the four metal's melting point temperature.

As we are trying to observe the flow pattern for any liquid-metal while not considering any particular type of matrix structure, so we kept the distribution of the radius following a normal distribution with a mean of 5 micrometers. The length is kept the same for all the pore and is equal to 10 micrometers. The full matrix is considered as 100*100, which is equal to 1 mm *1 mm area.

The flow is mostly due to the surface tension. However, in reality, it is common to apply a pressure difference between start and end to facilitate the flow. Here the pressure at the starting is given 10 Pa, and at the end edge, the pressure was given zero Pascal. This 10 Pa difference of pressure will force the flow along with its surface force.

Form the output data, graphs were plotted, and some parameters were observed to understand the flow. Section “RESULTS AND DISCUSSIONS” described on that.

4.4 FINDING THE RESISTANCE FOR FLOW THROUGH MICRO-PILLARED COOLING SYSTEM

As discussed in section three, problem one, the resistance of each cell is needed to be found to do the full-scale physics simulation. The full-scale physics simulation algorithm is described in section 4.1. The EXPNS works by considering the total body as a network of connections. Each of these connections has a conductivity that varies with the flow. The EXPNS was built in a way so that it can measure the resistance by its own and that was for a flow which has no mass loss due to evaporation or any other reason. The resistance measured by EXPNS is due to the already occupied fluid inside the pipe. When the proportion of this occupied fluid changes, then the resistance also changes. This process is mentioned elaborately in section 4.1. However, to solve this flow through the micro pillared cooling system, we would need to reconstruct this resistance measuring system as this model is different from that perspective.

Figure 11 shows a description of how nodes and connections are selected. The center point between four pillars (as like figure 11 (a)) is considered as a node. According to the description in section 4.1, a node is the point where four connections joints and virtue of a node is that it does not accumulate any fluid. Here when the system is in the steady-state condition, the node which is a point between any four cylinders also do not accumulate any fluid. The area between two such nodes is considered a connection or a cell for which resistance needed to be found. The description of EXPNS in section 4.1 described the working principle with the term conductance, which is nothing but the reciprocal of the resistance.

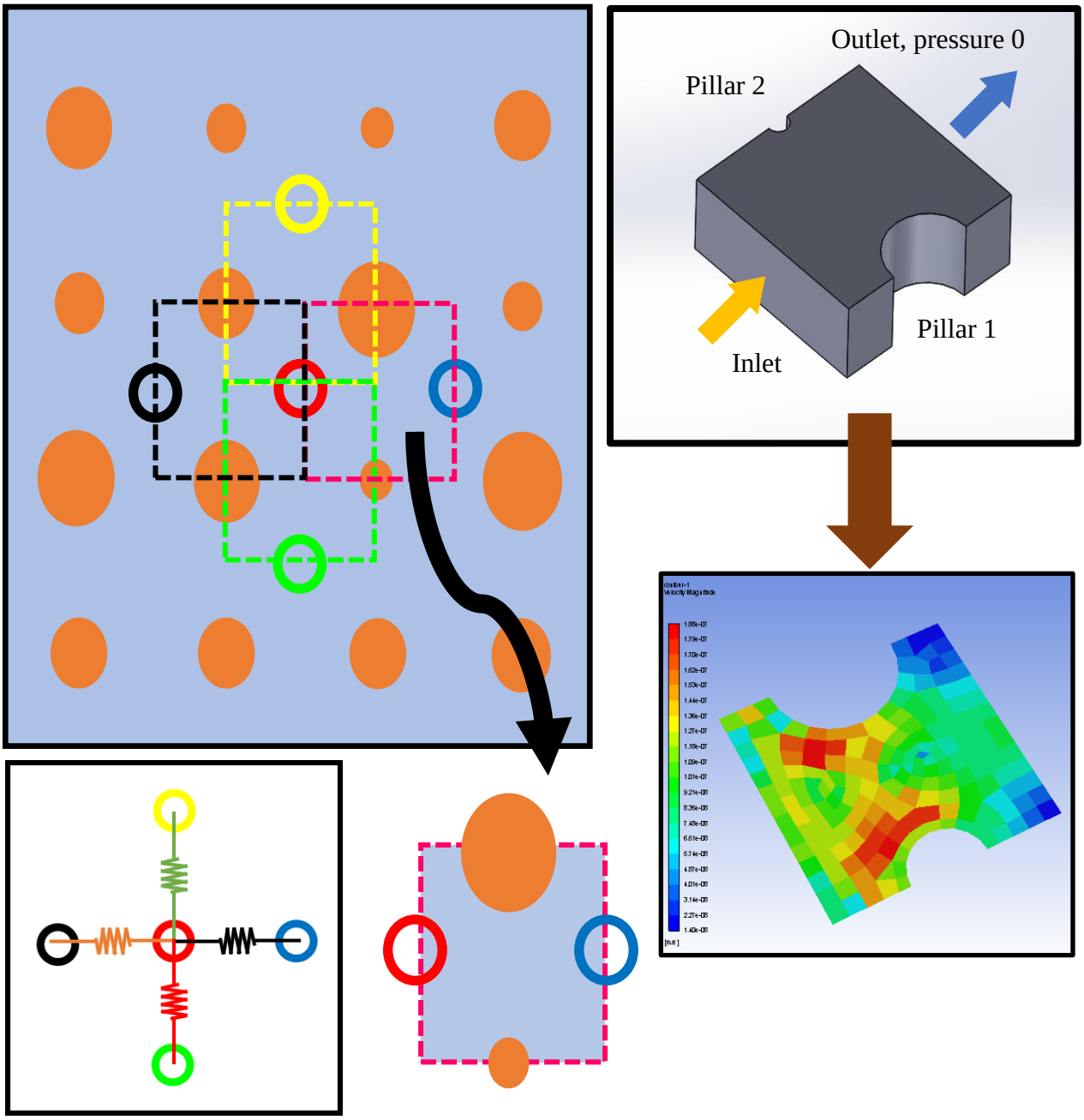

Figure 12: (a) Unit cells or connections for finding the resistance. (b) a 3d cad model of the cell (c) showing the Ansys output result contour

It was mentioned before that according to the paper [55] the optimal ratio of the parameters is as follows: $\frac{d}{h} \approx 0.4$ and $\frac{l}{d} \approx 3$. As we are only concern about the diameter, so we kept the other parameters constant and followed their finding. We considered the $h = 5\ \mu m$ and $l = 9\ \mu m$. The d should be around three micro-meters according to them. For the diameter, we considered a range from 1 to 5 micro-meter with one micro-meter increment. Which gives us five options for diameter. As inside one single cell, there are half of 2 cylinders, and the resistances are same if the diameter values are switched of any particular combination so there will be a total of 15 different combinations of a cell. For any of these cases, different height conditions must be considered as resistances changes with height. The height here is referring to the average height, and for the simulations, that average value is used for each case rather than considering a curved meniscus which will pose a high complexity in modeling while giving no benefit. The paper [55] showed that while finding the resistance excluding this consideration of the curved surface and considering the average height instead does not make a big difference. Now also from their work, it is known that for our scenario the average height will vary from 3 to 5 micro-meter. So, we considered a range from 3 to 5 micro-meter with 0.5 increment, which gives 5 different heights. So, the total number of combinations is now 5*15=75.

For CAD modeling, the software solid works were used. A macros script was constructed which serially made these CAD files instead of creating them individually in hand. Then they were imported to the simulation software Ansys. In the Ansys, we gave boundary conditions of the bottom, top, and cylindrical surfaces as the no-slip boundary condition. Even though the top surface is made of water, but that water is stagnant. For two sides, symmetric boundary condition was chosen. For the flow to be happening a pressure difference would be needed between the entrance and the exit surface. In reality, the flow happens due to the pressure difference created by

the water evaporation. If there was no heat applied, then after achieving steady-state, there will be no flow. All the point of the surface would have the same water pressure, and that would be equal to the atmospheric pressure. If heat is applied at a constant rate at the bottom surface, then water gets vapored and to fill the vacuum water rushes to that area. Due to flow, there is some pressure loss. When in a steady situation the amount of flow towards an area is equal to the flow out from the area plus the water getting evaporated from the area. Now flow will happen to that area only if that area has lower pressure than the surrounding area. The pressure of a cell directly contributes to the meniscus curvature and average water height of that cell. In reverse knowing the contact angle of the meniscus of a cell, it is possible to find the water pressure of that cell. We can use the formula shown in section 3 (problem 1): $\left(P_{vaper} - P_{liquide}\right) * (l^2 - \pi r^2) = 2\pi r\sigma \cos\theta$ While θ is the average contact angle. So, the lowest possible pressure will be when the contact angle is minimum. For our case, we calculated the lowest possible pressure in our surface by considering a cell having four cylinders with the highest diameter, and that is 5 micrometers. The minimum contact angle is considered 15 degrees as that is the amount for water and silicon oxide [55]. The surface tension is considered at 100 degree Celsius. In reality, the temperature at a steady-state could be less, but we are just considering an extreme situation to get an idea of water flow. The pressure difference is around 0.015 pascal for the highest and lowest point. For finding the resistance, we simulated each scenario with pressure difference ranging from 0.001 pascals to 0.015 pascals. So, in total, there were 15*75 simulations to be done. All these were done with Ansys fluent and atomization of Ansys was done with macros script. Figure 12 shows the applied boundary conditions.

CHAPTER 5: RESULTS AND DISCUSSIONS

5.1 VALIDATION OF EXPNS:

The method of validating the EXPNS was described in section 4.2. Here some of the comparisons of results from two methods are showed and discussed.

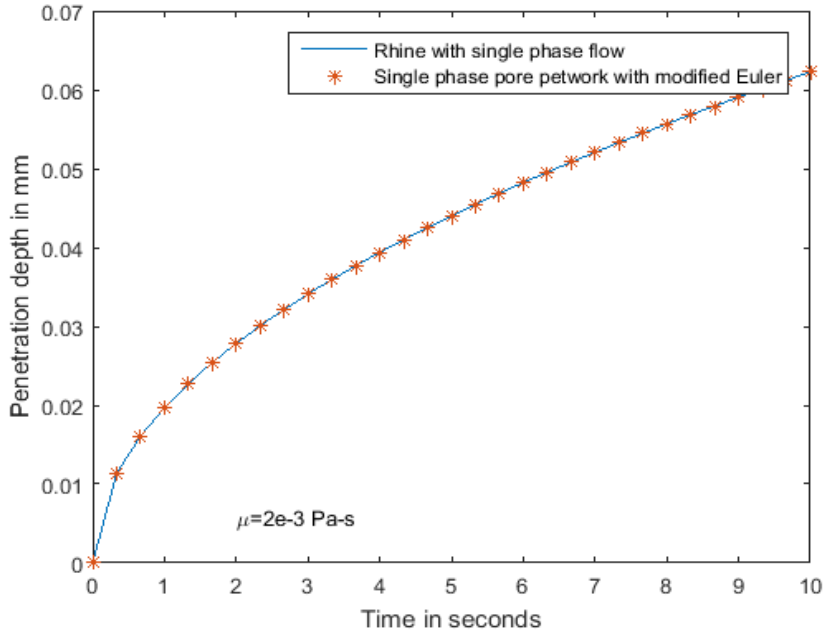

Figure 12: Average penetration depth for a single-phase flow with time

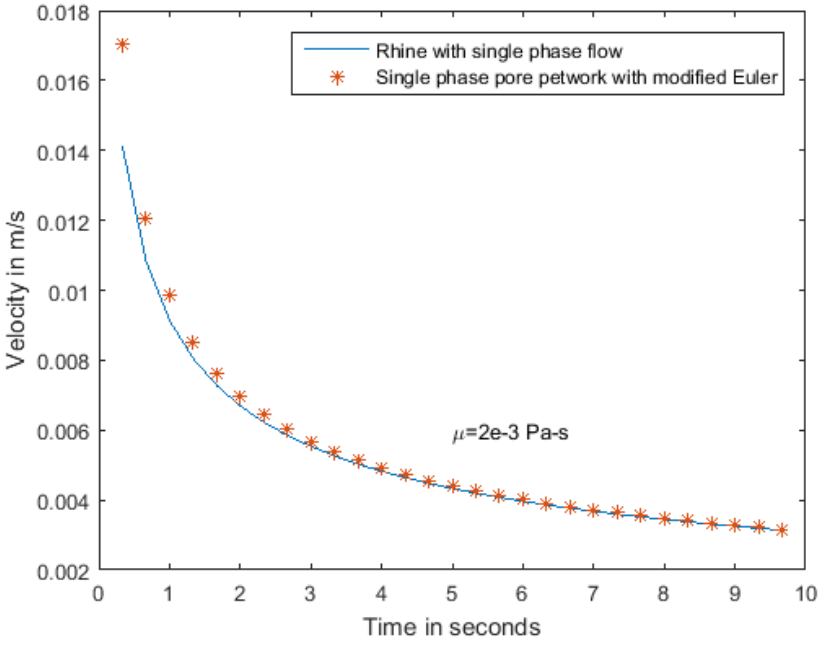

Figure 13: Average velocity for a single-phase flow with time

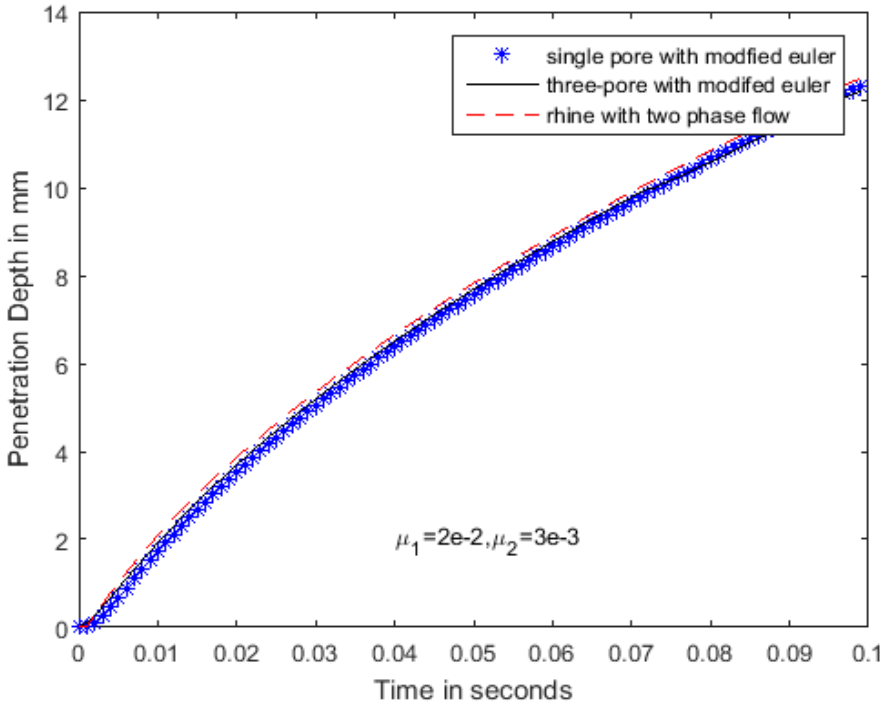

Figure 14: Average penetration depth for a two-phase flow with time

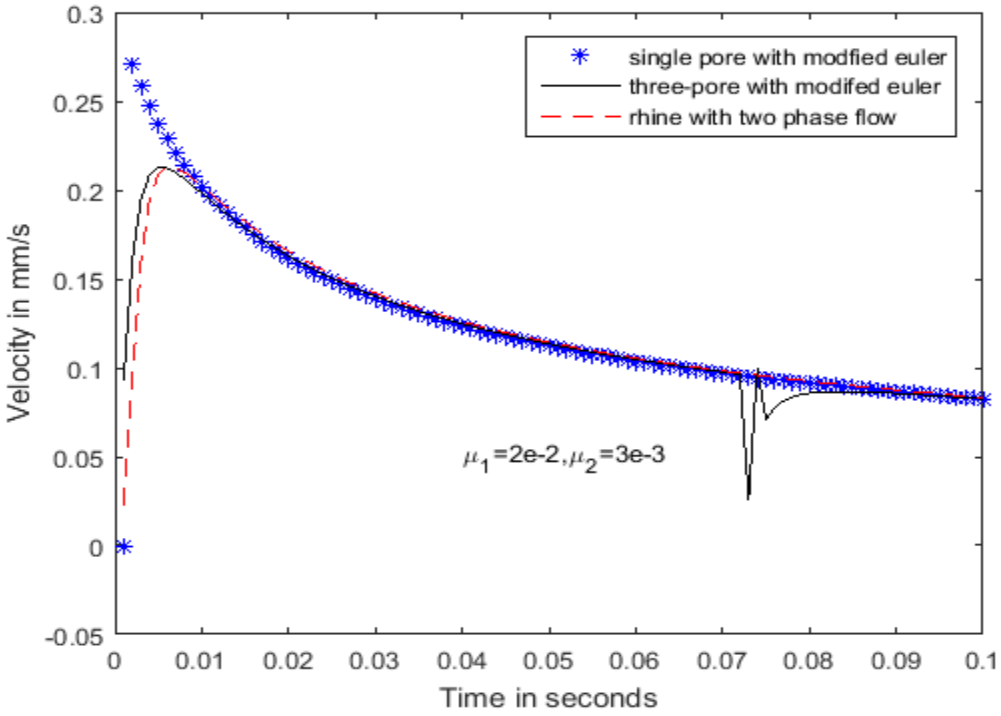

Figure 15: Average velocity for a two-phase flow with time

All the figures show the EXPNS simulation results have perfect similarity with the analytical established solution given by Rhine's equation. It provides the necessary proof of EXPNS reliability [77].

5.2 LIQUID METAL FLOW:

For observing the flow, two parameters were chosen: penetration depth and penetration rate. Both of this parameter were compared against time. Also, the maximum, minimum and average penetration and penetration rate was observed. Here is a random example of the flow pattern simulated by EXPNS for a better explanation of these parameters:

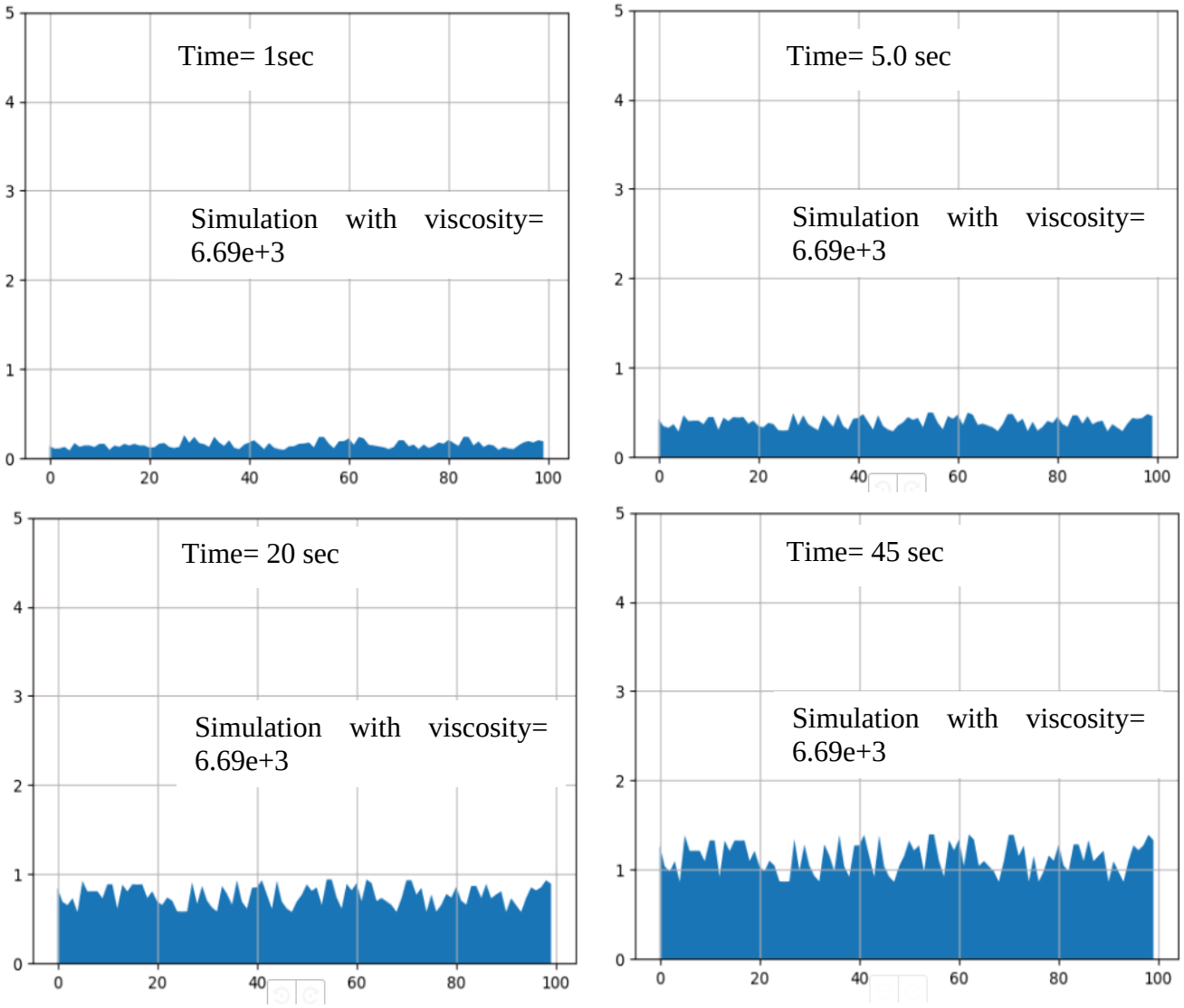

Figure 16: An example of flow simulation through porous media by EXPNS

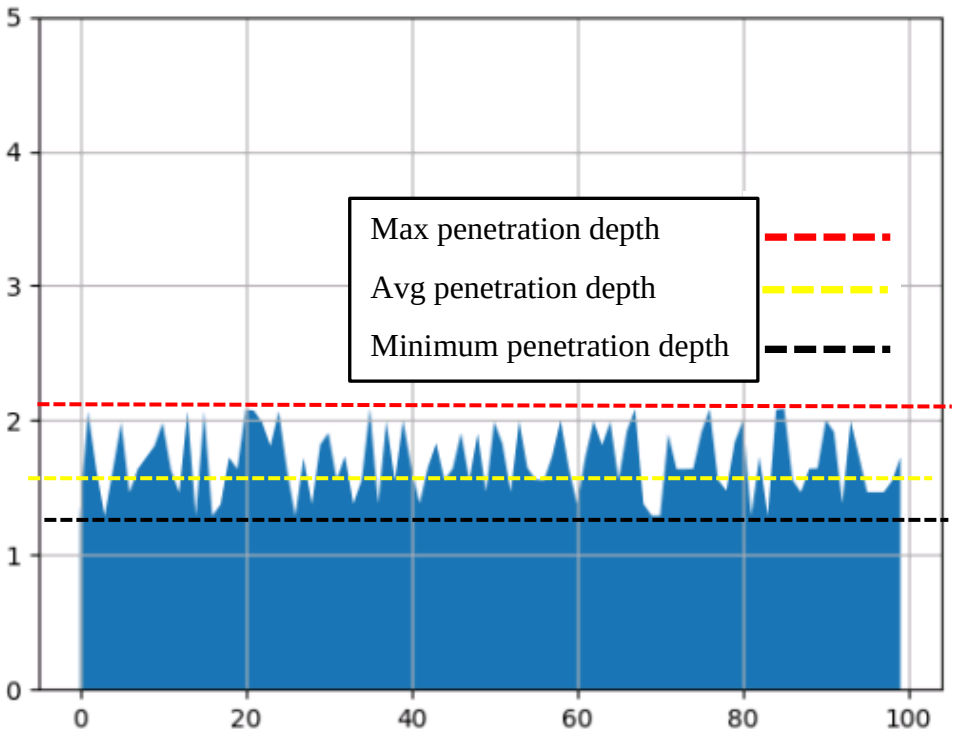

Figure 17: Maximum, minimum and average penetration depth

Penetration rates are derived from changes in penetration with time. For visualizing, these data of penetration depths and penetration rates are graphed against time. Two different temperature was chosen: one is the melting point temperature of the liquid, and another is 2300℃. This second temperature is higher than any of the metal's melting point temperature. The figures of penetration depth vs time and penetration rate vs time is given on the following pages.

TITANIUM (Ti) at melting point temperature [$1{,}668°C$]:

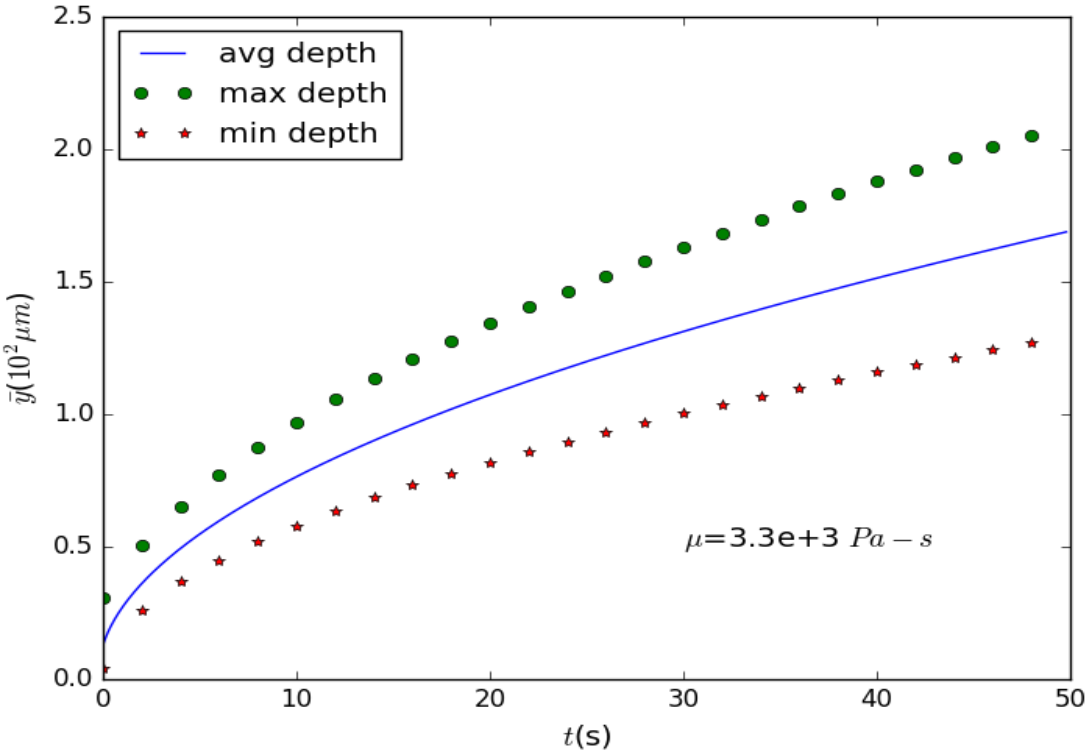

Figure 16: Penetration depth versus time for molten Titanium at melting point temperature

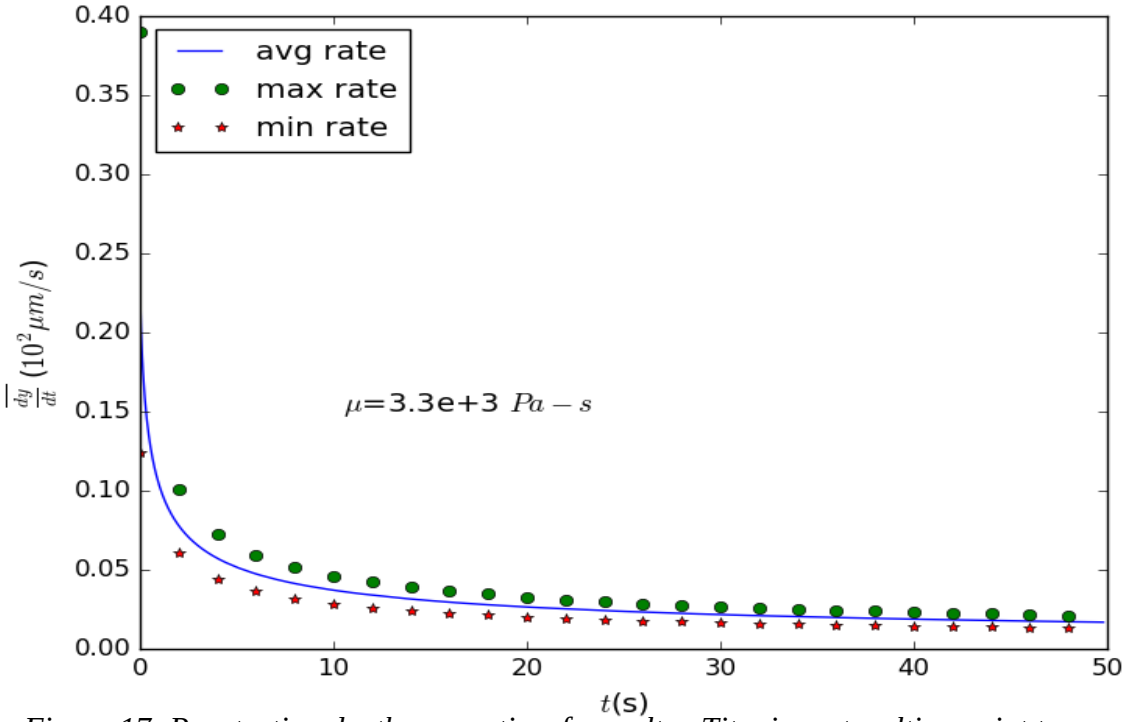

Figure 17: Penetration depth versus time for molten Titanium at melting point temperature

YTTRIUM (Y) at melting point temperature [1,526°C]:

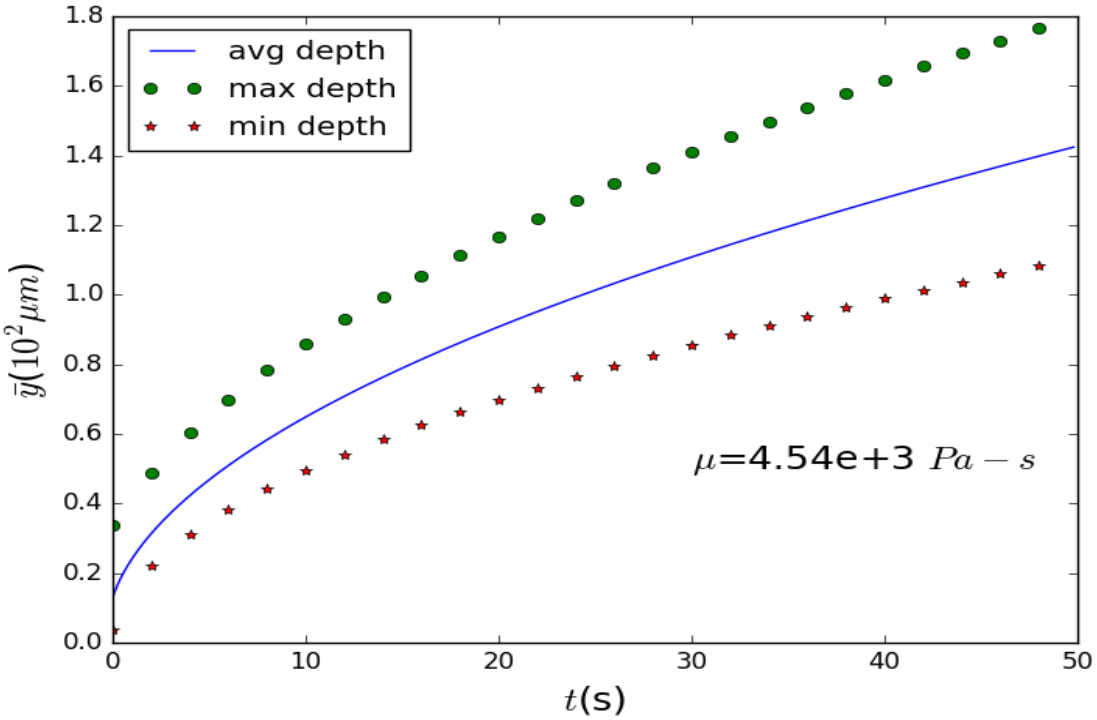

Figure 18: Penetration depth versus time for molten Yttrium at melting point temperature

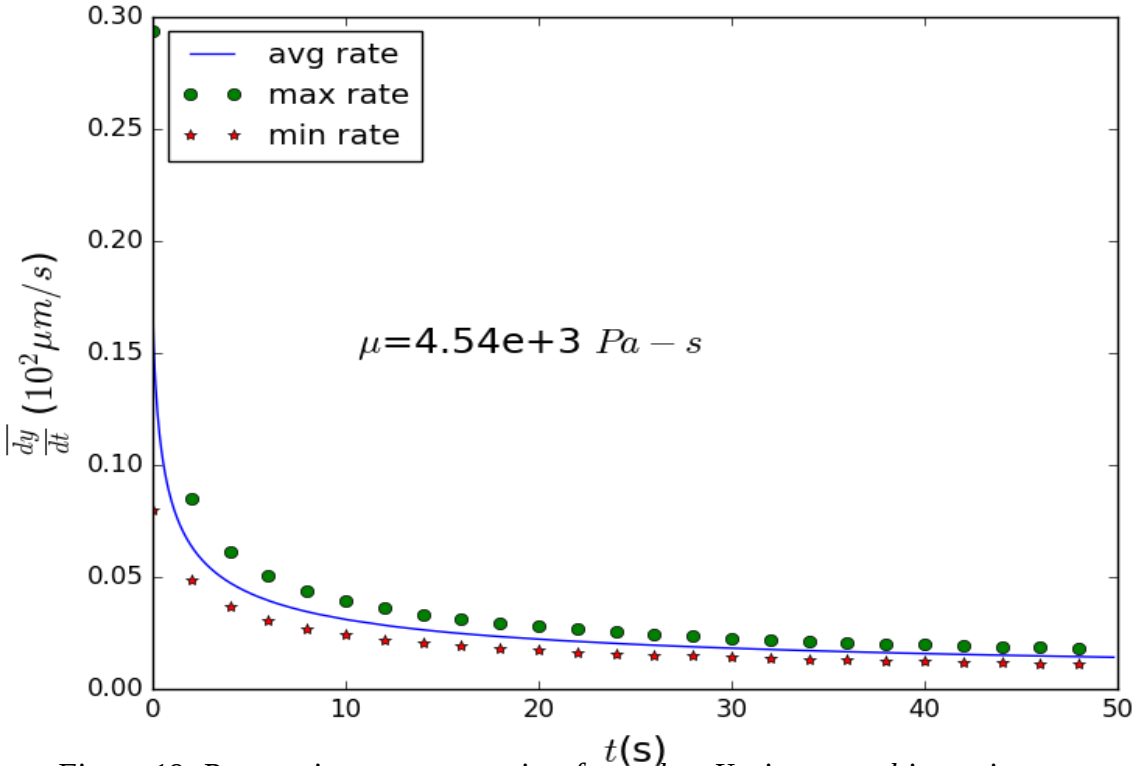

Figure 19: Penetration rate versus time for molten Yttrium at melting point temperature

ZIRCONIUM (Zr) at melting point temperature [$1{,}855°C$]:

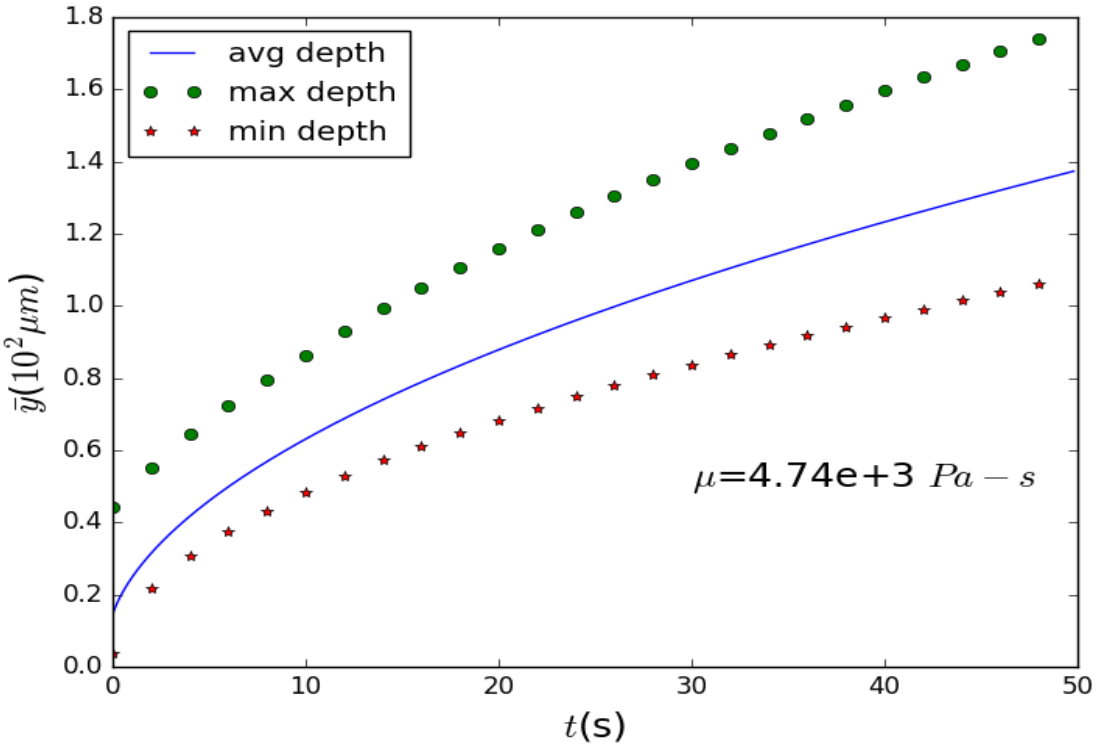

Figure 20: Penetration depth versus time for molten Zirconium at melting point temperature

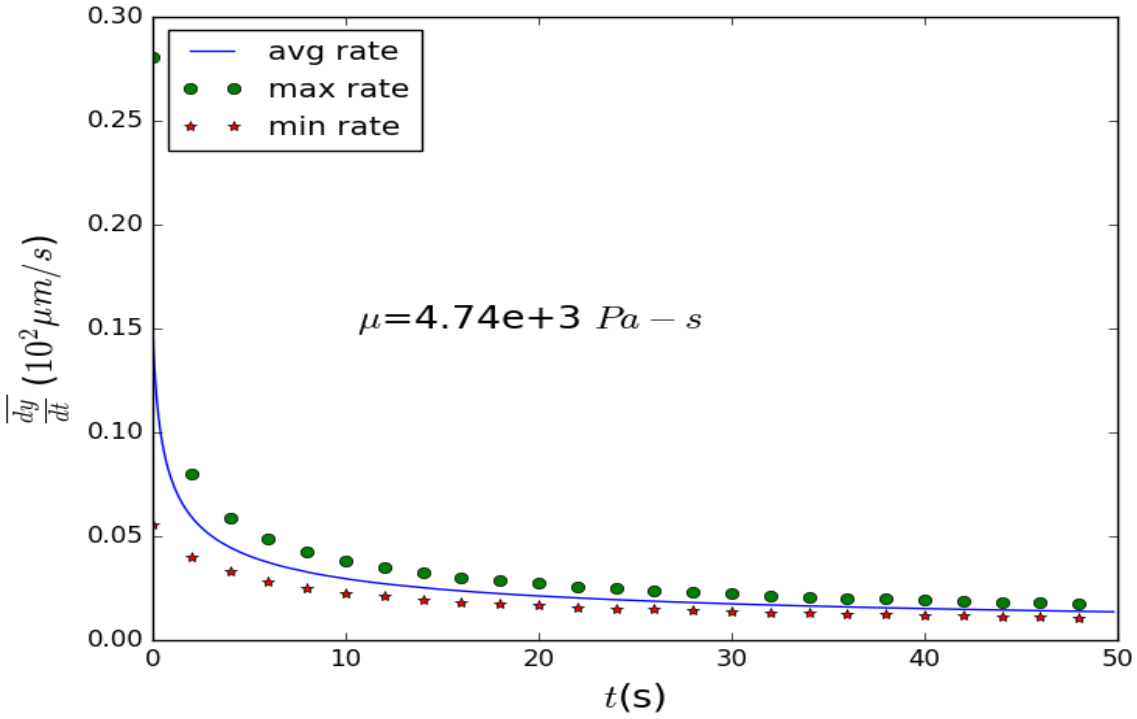

Figure 21: Penetration rate versus time for molten Zirconium at melting point temperature

HAFNIUM (Hf) at melting point temperature [$2,233°C$]:

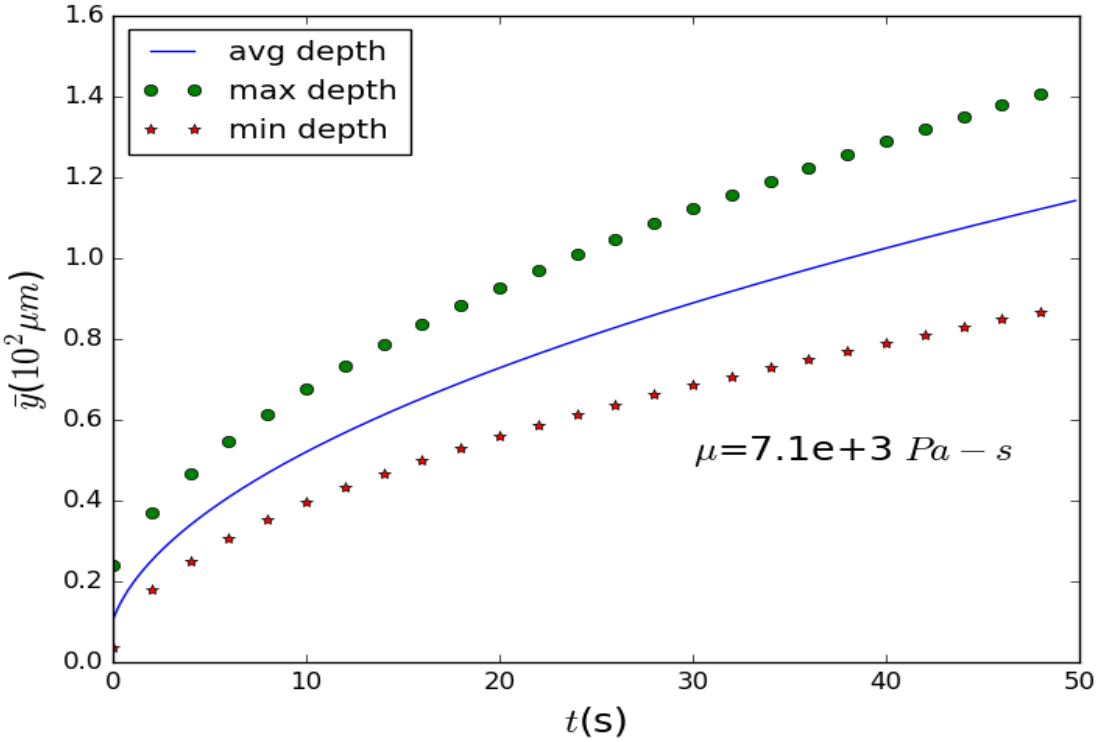

Figure 22: Penetration depth versus time for molten Hafnium at melting point temperature

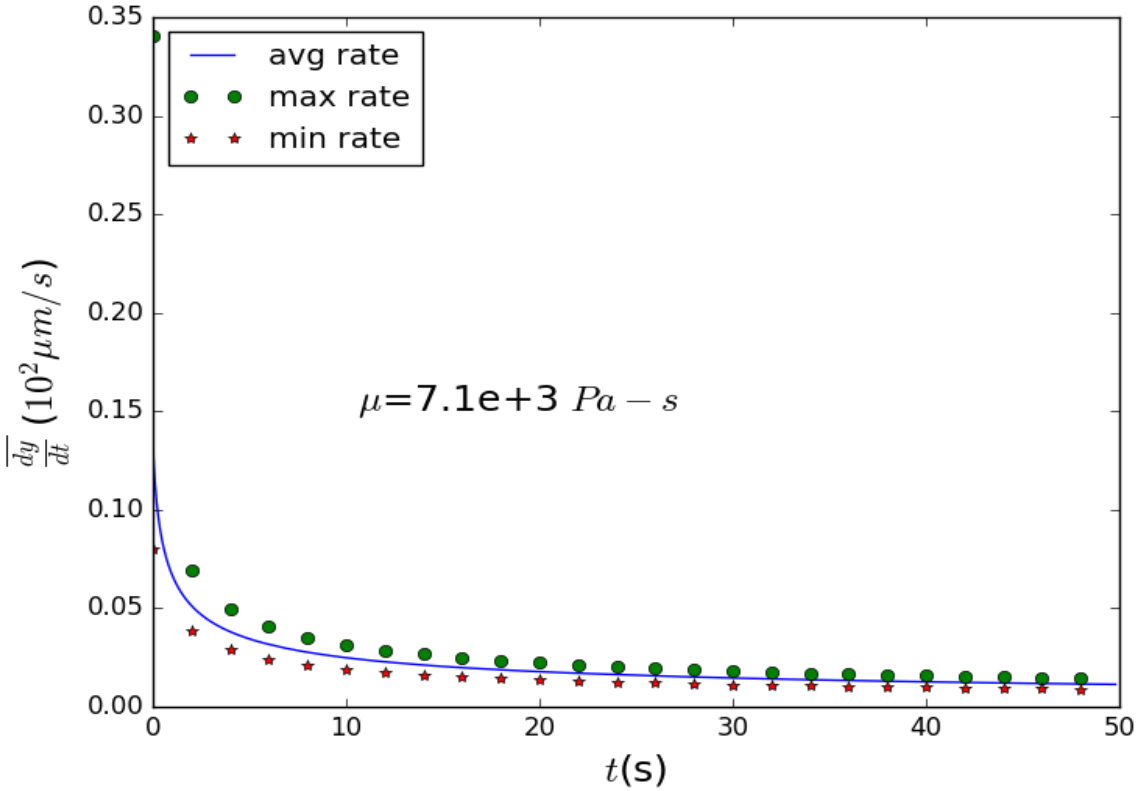

Figure 23: Penetration rate versus time for molten Hafnium at melting point temperature

TITANIUM (Ti) [2300℃]:

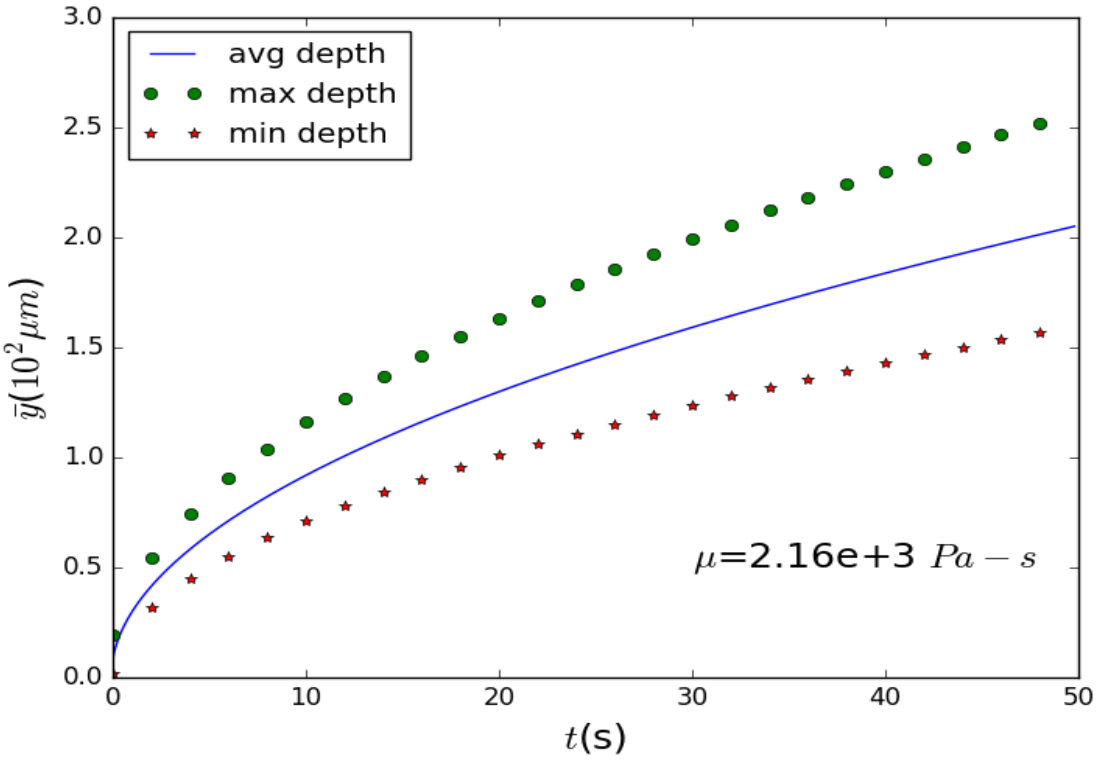

Figure 24: Penetration depth versus time for molten Titanium at 2300℃

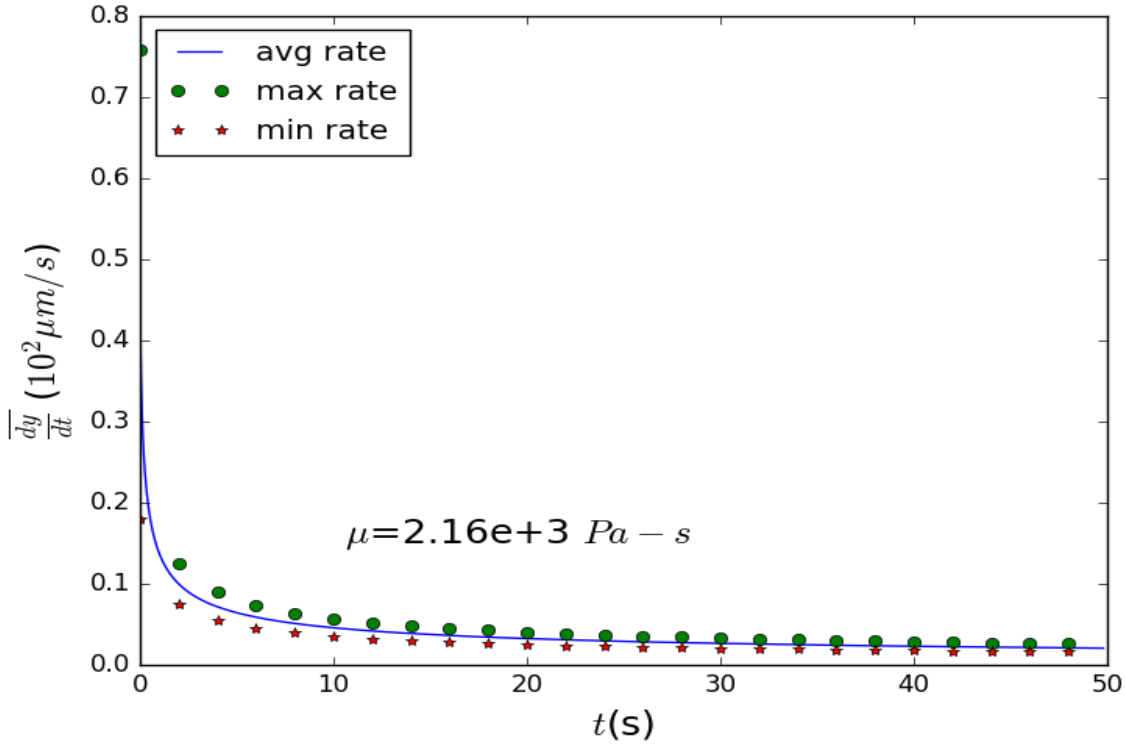

Figure 25: Penetration rate versus time for molten Titanium at 2300℃

YTTRIUM (Y) [2300℃]:

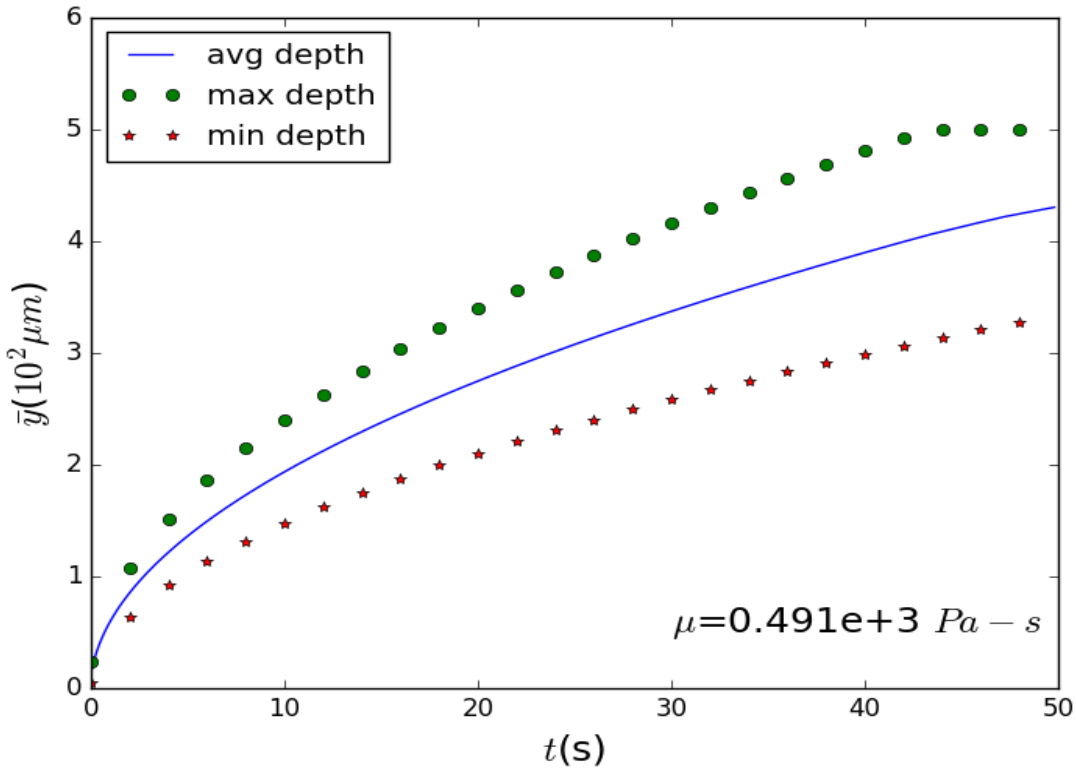

Figure 26: Penetration depth versus time for molten Yttrium at 2300℃

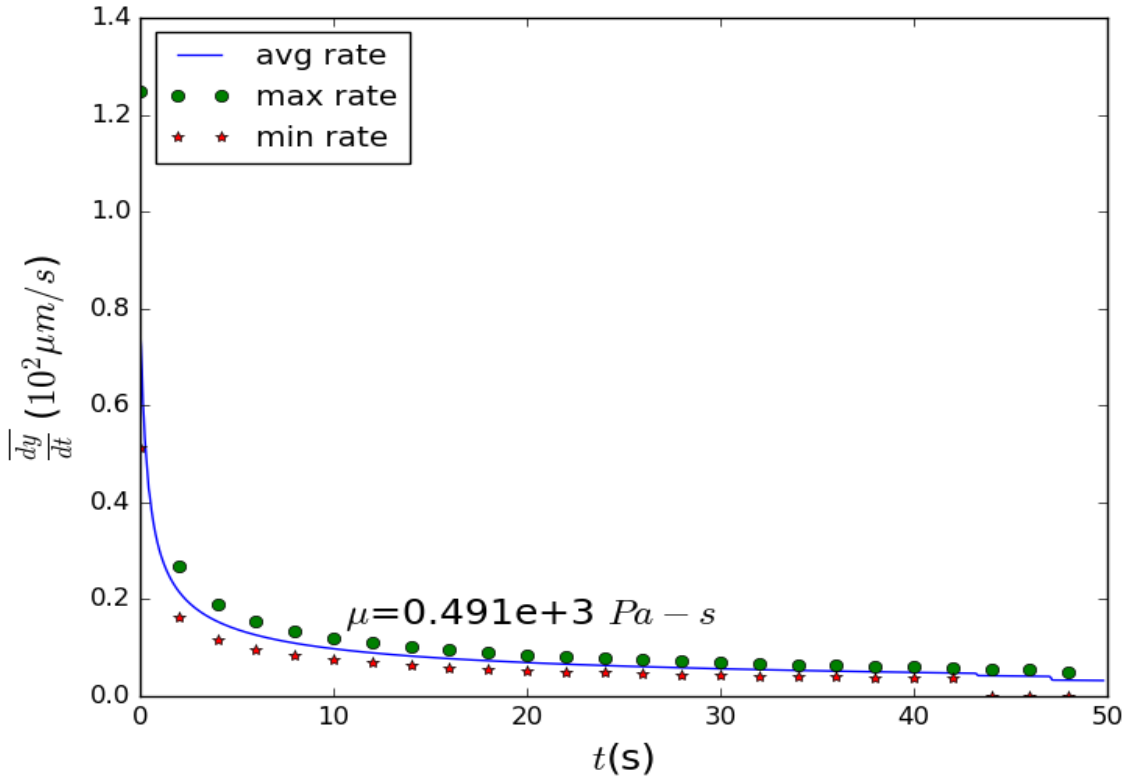

Figure 27: Penetration rate versus time for molten Yttrium at 2300℃

ZIRCONIUM (Zr) [2300℃]:

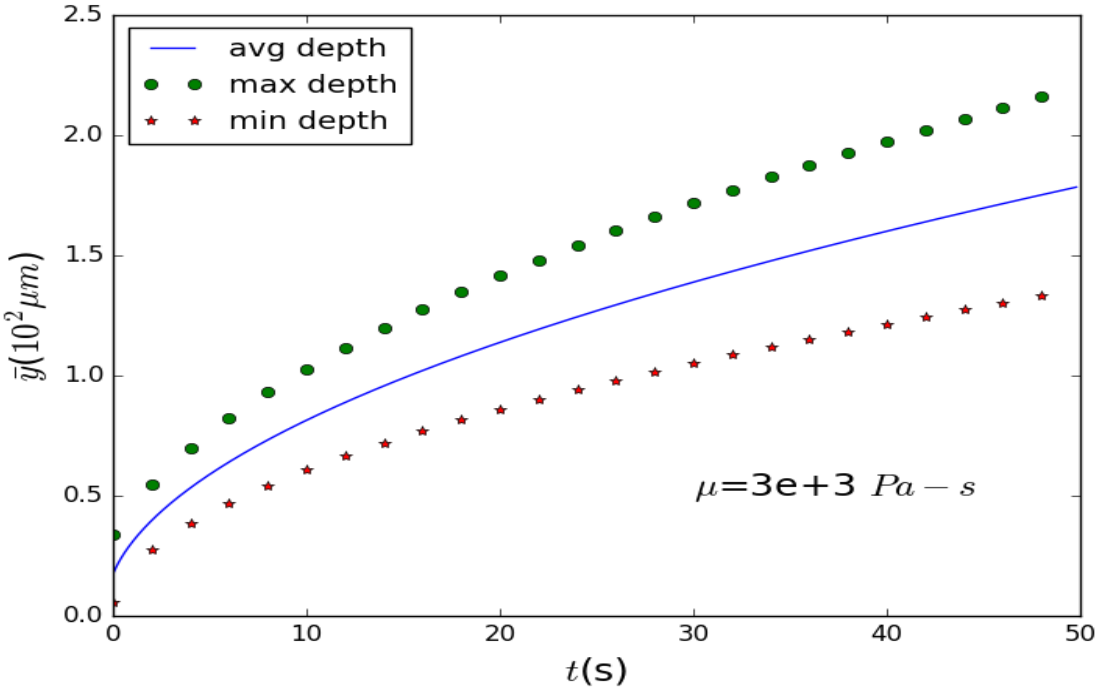

Figure 28: Penetration depth versus time for molten Zirconium at 2300℃

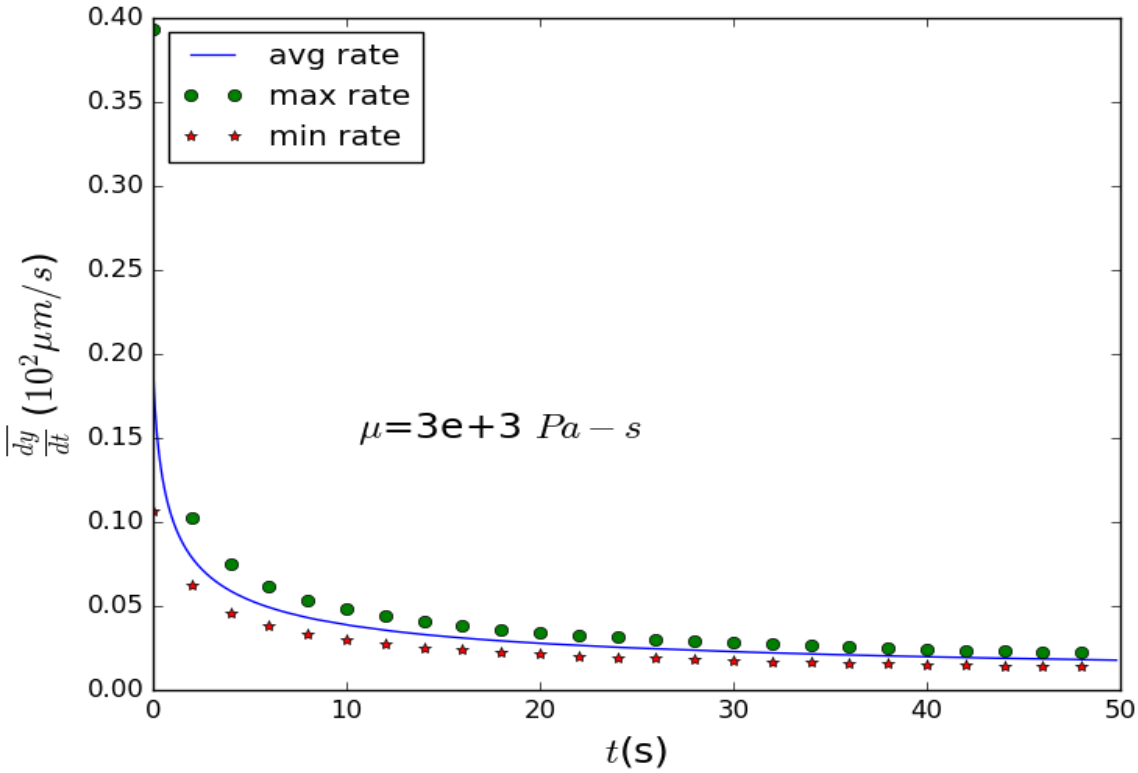

Figure 29: Penetration rate versus time for molten Zirconium at 2300℃

Hafnium (Hf) [2300℃]:

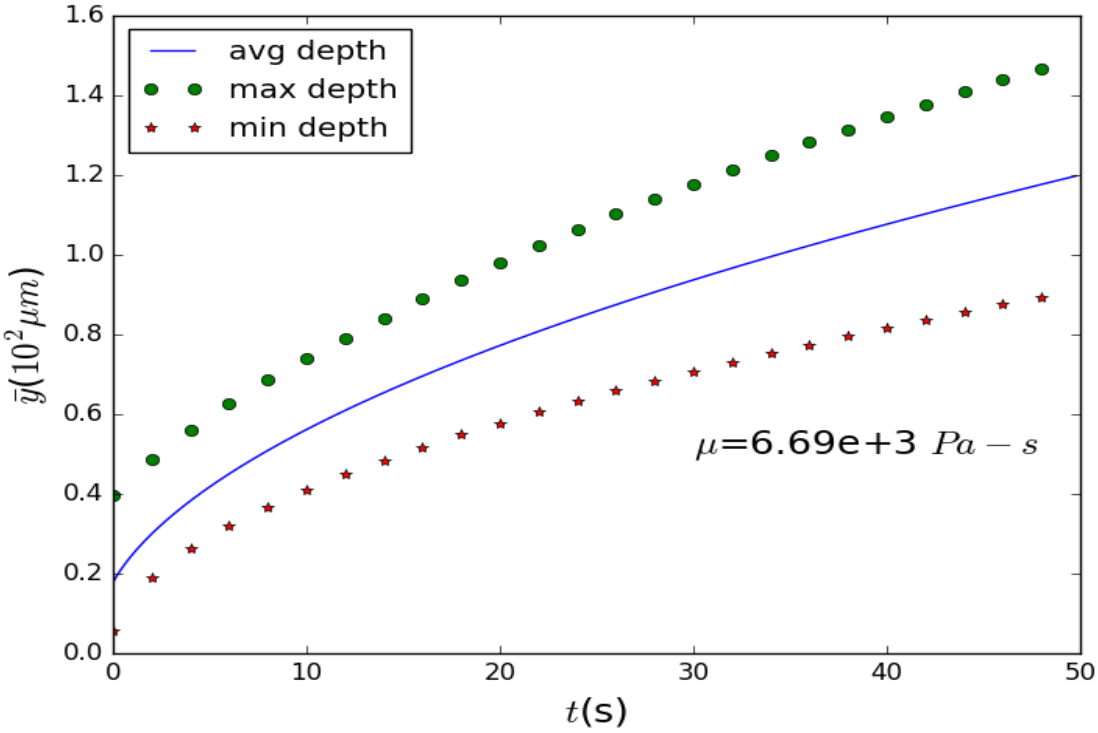

Figure 30: Penetration depth versus time for molten Hafnium at 2300℃

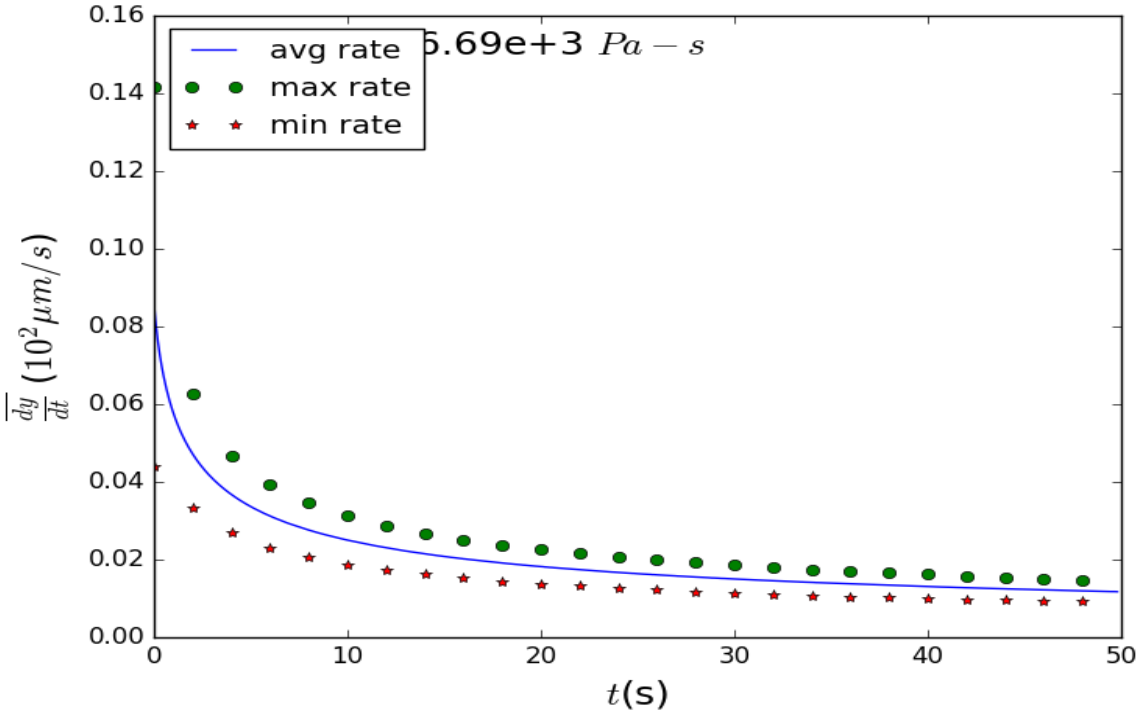

Figure 31: Penetration rate versus time for molten Hafnium at 2300℃

From all the penetration rate versus time graphs it is obvious that the rate decreases with time. The reason is nothing but fluid accumulation. As with the increment of time, more and more penetrating molten metal gets into the medium and so they create resistance to new incoming materials. The incoming new materials must move these preexisting metals to get into the pores. That means with the increment of time the resistances get higher and so the rate drops.

For all the cases, in general, the average penetration depth at 2300℃ at any time is higher than it was at its melting temperature for that time. The reason is apparent as with the increment of temperature the viscosity drops for most of the liquids and thus decrease the flow resistance, which helped to penetrate more than the case with higher viscosity. For the Hafnium, this difference is the lowest as its melting temperature is higher than others and near to the 2300℃ (2233℃).

5.3 RESISTANCE OF THE MICRO PILLARED COOLER WITH VARIABLE DIAMETERS:

As mentioned in the methodology section data has been generated for the conductance of different structures. In each structure 15 pressure differences were simulated and from that flow rate was got as output. Dividing that flow rate (volume flow rate) with the associative pressure gives the conductance. Thus a lookup chart is formulated for the conductance of different structures. Any data in between can be interpolated. Some of the specimens of that data are given below as graph.

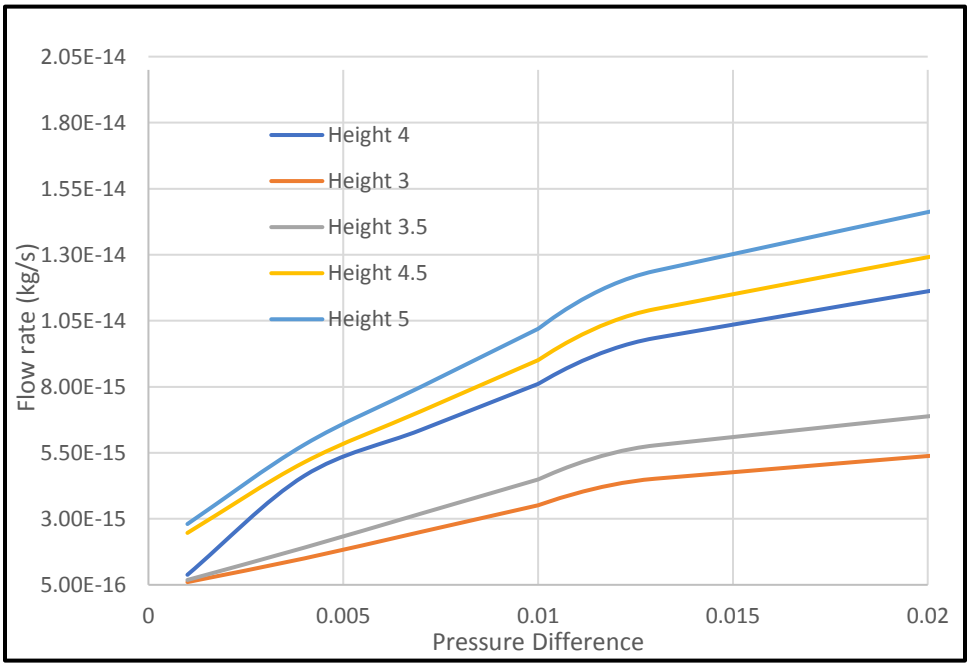

Figure 32: Graph of flow rate vs pressure difference induced

Figure 32 shows that the relation between the pressure difference and the flow rate (Kg/s) is almost linear. Which implies that a constant conductance can be calculated while considering the equation as $k = \frac{flow\ rate}{pressure\ difference}$. The graph above is for the structure which has one pillar with a diameter 1 micrometer and another 4 micrometers, and the height was considered three micro-meters.

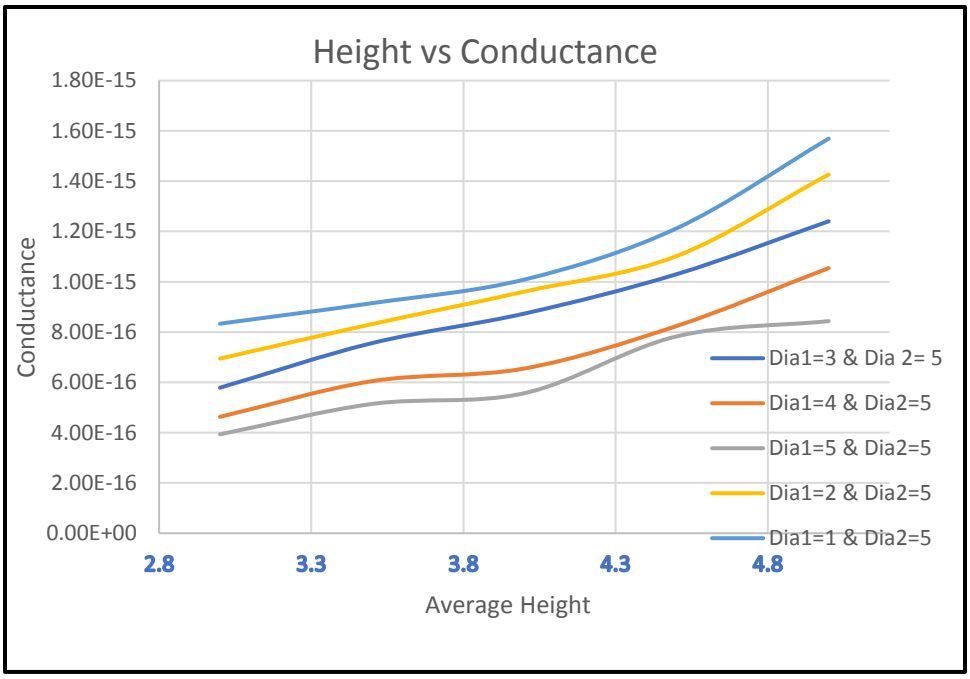

Figure 33: Graph of conductance vs pressure difference induced

This graph shows an example of the calculated conductance. Five structures are presented here with different diameters. All the diameter and height dimensions are in micrometers. With the increase of height, the conductance increases for all the cases, which is due to the direct cause of having more space. Also, with an increment of diameters on one side while another side is fixed the conductance decreases which also due to the same fact that cross-section is decreasing.

CHAPTER 6: CONCLUSION & FUTURE SCOPE

In this thesis, we have discussed the EXPNS and showed its application on molten metal flow. This flow simulation can help us to choose better matrix so that no bubble gets trapped inside and thus it can contribute to higher quality products. Also, expanding this work in 3 dimensions can help us to better understand the issue. This work does not include the possibility of heat transfer from the molten metal and associative volume inflammation of the matrix. Also, due to the heat transfer the temperature will decrease in the molten metal which will lead to a change in viscosity and surface tension. Considering these into the simulation will give us the opportunity to observe a more realistic situation and give us the advantage of making decisions based on that.

For the other work, we have lots of future scopes. It was done to understand the flow resistance in a different structure. Now that we have the data set, we can use it for simulating the flow by using the EXPNX. As the EXPNS needs to calculate the resistance in every step and in the case of micro-pillared cooling system it is not possible to get it by considering the connections as a pipe; we can use the chart as a replacement for that. Simulating the micro-pillared cooling structure, we will able to find a more efficient structure for transferring more heat. This advancement in heat removal will allow building more fast microprocessors as heat removal is the bottleneck of that problem.

REFERENCES

[1] "What Is High-Performance Computing (HPC)? | How It Works | NetApp." [Online]. Available: https://www.netapp.com/us/info/what-is-high-performance-computing.aspx. [Accessed: 12-Jun-2019].

[2] S. Cant, "High-performance computing in computational fluid dynamics: progress and challenges," *Philos. Trans. R. Soc. London. Ser. A Math. Phys. Eng. Sci.*, vol. 360, no. 1795, pp. 1211–1225, Jun. 2002.

[3] C. Wagner, A. Shishkin, and O. Shishkina, "The use of Direct Numerical Simulations for solving industrial flow problems," Springer, Dordrecht, 2011, pp. 397–404.

[4] "Message Passing Interface (MPI)." [Online]. Available: https://computing.llnl.gov/tutorials/mpi/. [Accessed: 12-Jun-2019].

[5] "High performance Linux clustering, Part 2: Build a working cluster." [Online]. Available: https://www.ibm.com/developerworks/library/l-cluster2/index.html. [Accessed: 12-Jun-2019].

[6] M. D. Hill and M. R. Marty, "Amdahl's law in the multicore era," *Computer (Long. Beach. Calif).*, vol. 41, no. 7, pp. 33–38, 2008.

[7] Gene M. Amdahl, "Validity of the single processor approach to achieving large scale computing capabilities," *AFIPS spring Jt. Comput. Conf.*, 1967.

[8] J. L. Gustafson, "Reevaluating Amdahl's law," *Commun. ACM*, vol. 31, no. 5, pp. 532–533, 1988.

[9] W. Gropp, E. Lusk, N. Doss, and A. Skjellum, "A high-performance, portable

implementation of the MPI message passing interface standard," *Parallel Comput.*, vol. 22, no. 6, pp. 789–828, Sep. 1996.

[10] J. JáJá, "An Introduction to Parallel Algorithms." 1992.

[11] "3.4 Topology." [Online]. Available: https://www.phy.ornl.gov/csep/ca/node22.html. [Accessed: 18-Jun-2019].

[12] K. Hwang and A. Faye, "Computer architecture and parallel processing." McGraw-Hill,New York, NY, USA, 01-Jan-1984.

[13] P. Architectures, "Message Passing Fundamentals," *Access*, pp. 1–202, 2001.

[14] Y. Igarashi, T. Altman, M. Funada, and B. Kamiyama, "Parallel and Distributed Computing," *Computing*, pp. 271–282, 2014.

[15] V. Kumar, A. Grama, A. Gupta, and G. Karypis, *Introduction to parallel computing : design and analysis of algorithms*. Benjamin/Cummings Pub. Co, 1994.

[16] "NUMA Deep Dive Part 1: From UMA to NUMA - frankdenneman.nl." [Online]. Available: https://frankdenneman.nl/2016/07/07/numa-deep-dive-part-1-uma-numa/. [Accessed: 18-Jun-2019].

[17] C. Lameter and Christoph, "NUMA (Non-Uniform Memory Access): An Overview," *Queue*, vol. 11, no. 7, p. 40, Jul. 2013.

[18] A. Ali and K. S. Syed, "An Outlook of High Performance Computing Infrastructures for Scientific Computing," *Adv. Comput.*, vol. 91, pp. 87–118, Jan. 2013.

[19] L. Dagum and R. Menon, "OpenMP: an industry standard API for shared-memory programming," *IEEE Comput. Sci. Eng.*, vol. 5, no. 1, pp. 46–55, 1998.

[20] H. C. Edwards and C. R. Trott, “Kokkos: Enabling Performance Portability Across Manycore Architectures,” in *2013 Extreme Scaling Workshop (xsw 2013)*, 2013, pp. 18–24.

[21] J. Shalf, S. Dosanjh, and J. Morrison, “Exascale Computing Technology Challenges,” Springer, Berlin, Heidelberg, 2011, pp. 1–25.

[22] C. A. Mack, “Fifty Years of Moore’s Law,” *IEEE Trans. Semicond. Manuf.*, vol. 24, no. 2, pp. 202–207, May 2011.

[23] M. Behnia, L. Maguire, and G. Morrison, “Cooling problems and thermal issues in high power electronics - a multi faceted design approach,” in *5th International Conference on Thermal and Mechanical Simulation and Experiments in Microelectronics and Microsystems, 2004. EuroSimE 2004. Proceedings of the*, pp. 519–526.

[24] B. Agostini, M. Fabbri, J. E. Park, L. Wojtan, J. R. Thome, and B. Michel, “State of the Art of High Heat Flux Cooling Technologies,” *Heat Transf. Eng.*, vol. 28, no. 4, pp. 258–281, Apr. 2007.

[25] P. Wilson and P. Wilson, “Power Supplies,” *Circuit Des. Companion*, pp. 321–364, Jan. 2017.

[26] “Synthetic jets for forced air cooling of electronics | Electronics Cooling.” [Online]. Available: https://www.electronics-cooling.com/2007/05/synthetic-jets-for-forced-air-cooling-of-electronics/. [Accessed: 25-May-2019].

[27] L. Jiang *et al.*, “Closed-loop electroosmotic microchannel cooling system for VLSI circuits,” *IEEE Trans. Components Packag. Technol.*, vol. 25, no. 3, pp. 347–355, 2002.

[28] A. Poachaiyapoom, R. Leardkun, J. Mounkong, and S. Wongwises, “Miniature vapor

compression refrigeration system for electronics cooling," *Case Stud. Therm. Eng.*, vol. 13, p. 100365, Mar. 2019.

[29] S. Adera, D. Antao, R. Raj, and E. N. Wang, "Design of micropillar wicks for thin-film evaporation," *Int. J. Heat Mass Transf.*, vol. 101, pp. 280–294, Oct. 2016.

[30] S. Ravi, D. Horner, and S. Moghaddam, "Monoporous micropillar wick structures, I-Mass transport characteristics," *Appl. Therm. Eng.*, vol. 73, no. 1, pp. 1371–1377, Dec. 2014.

[31] R. Ranjan, A. Patel, S. V. Garimella, and J. Y. Murthy, "Wicking and thermal characteristics of micropillared structures for use in passive heat spreaders," *Int. J. Heat Mass Transf.*, vol. 55, no. 4, pp. 586–596, 2012.

[32] Y. Zhu, D. S. Antao, Z. Lu, S. Somasundaram, T. Zhang, and E. N. Wang, "Prediction and Characterization of Dry-out Heat Flux in Micropillar Wick Structures," *Langmuir*, vol. 32, no. 7, pp. 1920–1927, 2016.

[33] D. Horner, S. Ravi, and S. Moghaddam, "Monoporous micropillar wick structures, II-optimization & theoretical limits," *Appl. Therm. Eng.*, vol. 73, no. 1, pp. 1378–1386, Dec. 2014.

[34] S. Somasundaram *et al.*, "Thermal design optimization of evaporator micropillar wicks," *Int. J. Therm. Sci.*, vol. 134, pp. 179–187, Dec. 2018.

[35] L. Zhang *et al.*, "Characterization of thin film evaporation in micropillar wicks using micro-Raman spectroscopy," *Appl. Phys. Lett.*, vol. 113, no. 16, p. 163701, Oct. 2018.

[36] "The Future of Metal Is in Matrix Composites." [Online]. Available: https://www.machinedesign.com/materials/future-metal-matrix-composites. [Accessed:

16-Aug-2019].

[37] S. N. Trinh and S. Sastry, “Processing and Properties of Metal Matrix Composites,” p. 17, 2016.

[38] M. D. Hayat, H. Singh, Z. He, and P. Cao, “Titanium metal matrix composites: An overview,” *Compos. Part A Appl. Sci. Manuf.*, vol. 121, pp. 418–438, Jun. 2019.

[39] C. S. Vidyasagar and D. B. Karunakar, “Development of 2024 AA-Yttrium composites by Spark Plasma Sintering,” *IOP Conf. Ser. Mater. Sci. Eng.*, vol. 346, p. 012050, Apr. 2018.

[40] M. Madhusudhan, G. J. Naveen, and K. Mahesha, “Mechanical Characterization of AA7068-ZrO2 reinforced Metal Matrix Composites,” *Mater. Today Proc.*, vol. 4, no. 2, pp. 3122–3130, Jan. 2017.

[41] V. Joekar-Niasar, S. M. Hassanizadeh, and A. Leijnse, “Insights into the Relationships Among Capillary Pressure, Saturation, Interfacial Area and Relative Permeability Using Pore-Network Modeling,” *Transp. Porous Media*, vol. 74, no. 2, pp. 201–219, Sep. 2008.

[42] Q. Yu, Y. Liu, X. Liu, D. Yao, and Y. Yu, “Experimental study on seepage flow patterns in heterogeneous low-permeability reservoirs,” *J. Pet. Explor. Prod. Technol.*, vol. 8, no. 2, pp. 589–596, Jun. 2018.

[43] J. G. Hoffmann, R. Echigo, H. Yoshida, and S. Tada, “Experimental study on combustion in porous media with a reciprocating flow system,” *Combust. Flame*, vol. 111, no. 1–2, pp. 32–46, Oct. 1997.

[44] M. T. van Genuchten and P. J. Wierenga, “Mass Transfer Studies in Sorbing Porous Media I. Analytical Solutions1,” *Soil Sci. Soc. Am. J.*, vol. 40, no. 4, p. 473, 1976.

[45] M. J. Blunt, “Flow in porous media — pore-network models and multiphase flow,” *Curr. Opin. Colloid Interface Sci.*, vol. 6, no. 3, pp. 197–207, Jun. 2001.

[46] J. T. Gostick, M. A. Ioannidis, M. W. Fowler, and M. D. Pritzker, “Pore network modeling of fibrous gas diffusion layers for polymer electrolyte membrane fuel cells,” *J. Power Sources*, vol. 173, no. 1, pp. 277–290, Nov. 2007.

[47] R. Glantz and M. Hilpert, “Capillary Displacement in Totally Wetting And Infinitely Long Right Prisms,” *Multiscale Model. Simul.*, vol. 9, no. 4, pp. 1765–1800, Oct. 2011.

[48] J. Hinebaugh, Z. Fishman, and A. Bazylak, “Unstructured Pore Network Modeling with Heterogeneous PEMFC GDL Porosity Distributions,” *J. Electrochem. Soc.*, vol. 157, no. 11, p. B1651, Nov. 2010.

[49] P. H. Valvatne and M. J. Blunt, “Predictive pore-scale modeling of two-phase flow in mixed wet media,” *Water Resour. Res.*, vol. 40, no. 7, Jul. 2004.

[50] M. Sahimi, “Fractal and superdiffusive transport and hydrodynamic dispersion in heterogeneous porous media,” *Transp. Porous Media*, vol. 13, no. 1, pp. 3–40, Oct. 1993.

[51] P. P. Mukherjee, Q. Kang, and C.-Y. Wang, “Pore-scale modeling of two-phase transport in polymer electrolyte fuel cells—progress and perspective,” *Energy Environ. Sci.*, vol. 4, no. 2, pp. 346–369, Feb. 2011.

[52] Y. Zhu, P. J. Fox, and J. P. Morris, “A pore-scale numerical model for flow through porous media,” *Int. J. Numer. Anal. Methods Geomech.*, vol. 23, no. 9, pp. 881–904, Aug. 1999.

[53] R. Ranjan, A. Patel, S. V. Garimella, and J. Y. Murthy, “Wicking and thermal characteristics of micropillared structures for use in passive heat spreaders,” *Int. J. Heat Mass Transf.*, vol.

55, no. 4, pp. 586–596, 2012.

[54] S. Adera, D. Antao, R. Raj, and E. N. Wang, “Design of micropillar wicks for thin-film evaporation,” *Int. J. Heat Mass Transf.*, vol. 101, pp. 280–294, 2016.

[55] Y. Zhu, D. S. Antao, Z. Lu, S. Somasundaram, T. Zhang, and E. N. Wang, “Prediction and Characterization of Dry-out Heat Flux in Micropillar Wick Structures,” *Langmuir*, vol. 32, no. 7, pp. 1920–1927, Feb. 2016.

[56] R. Xiao, R. Enright, and E. N. Wang, “Prediction and Optimization of Liquid Propagation in Micropillar Arrays,” *Langmuir*, vol. 26, no. 19, pp. 15070–15075, 2010.

[57] A. Aziz, “A similarity solution for laminar thermal boundary layer over a flat plate with a convective surface boundary condition,” *Commun. Nonlinear Sci. Numer. Simul.*, vol. 14, no. 4, pp. 1064–1068, Apr. 2009.

[58] T. Reports, “c,” no. November, 2010.

[59] J. Ghaboussi and E. L. Wilson, *International journal for numerical methods in engineering.*, vol. 5, no. 3. John Wiley & Sons, 1969.

[60] K. R. RAJAGOPAL, “ON A HIERARCHY OF APPROXIMATE MODELS FOR FLOWS OF INCOMPRESSIBLE FLUIDS THROUGH POROUS SOLIDS,” *Math. Model. Methods Appl. Sci.*, vol. 17, no. 02, pp. 215–252, Feb. 2007.

[61] G. Dagan, “Models of groundwater flow in statistically homogeneous porous formations,” *Water Resour. Res.*, vol. 15, no. 1, pp. 47–63, Feb. 1979.

[62] L. Chen, L. Zhang, Q. Kang, H. S. Viswanathan, J. Yao, and W. Tao, “Nanoscale simulation of shale transport properties using the lattice Boltzmann method: Permeability and

diffusivity," *Sci. Rep.*, vol. 5, pp. 1–8, 2015.

[63] S. Nickerson, Y. Shu, D. Zhong, C. Könke, and A. Tandia, "Permeability of porous ceramics by X-ray CT image analysis," *Acta Mater.*, vol. 172, pp. 121–130, Jun. 2019.

[64] "Shokri Research Group at Boston University." [Online]. Available: https://personalpages.manchester.ac.uk/staff/nima.shokri/DynamicsImmiscible.html. [Accessed: 04-Aug-2019].

[65] A. T. Krummel, S. S. Datta, S. Münster, and D. A. Weitz, "Visualizing multiphase flow and trapped fluid configurations in a model three-dimensional porous medium," Jan. 2013.

[66] "Dynamics of Fluids in Porous Media - Google Play." [Online]. Available: https://play.google.com/books/reader?id=fBMeVSZ_3u8C&hl=en_US&pg=GBS.PR18.w.0.1.15. [Accessed: 04-Aug-2019].

[67] "Fundamentals of Fluid Flow in Porous Media - Special Core Analysis & EOR Laboratory | PERM Inc." [Online]. Available: http://perminc.com/resources/fundamentals-of-fluid-flow-in-porous-media/. [Accessed: 04-Aug-2019].

[68] R. G. Larson, L. E. Scriven, and H. T. Davis, "Percolation theory of two phase flow in porous media," *Chem. Eng. Sci.*, vol. 36, no. 1, pp. 57–73, Jan. 1981.

[69] C. J. Van Duijn, J. Molenaar, and M. J. De Neef, "The effect of capillary forces on immiscible two-phase flow in heterogeneous porous media," *Transp. Porous Media*, vol. 21, no. 1, pp. 71–93, Oct. 1995.

[70] L. D. McKay, J. A. Cherry, R. C. Bales, M. T. Yahya, and C. P. Gerba, "A field example of bacteriophage as tracers of fracture flow," *Environ. Sci. Technol.*, vol. 27, no. 6, pp.

1075–1079, Jun. 1993.

[71] A. A. Keller, S. Sirivithayapakorn, and C. V. Chrysikopoulos, “Early breakthrough of colloids and bacteriophage MS2 in a water-saturated sand column,” *Water Resour. Res.*, vol. 40, no. 8, Aug. 2004.

[72] K.-M. Yao, M. T. Habibian, and C. R. O’Melia, “Water and waste water filtration. Concepts and applications,” *Environ. Sci. Technol.*, vol. 5, no. 11, pp. 1105–1112, Nov. 1971.

[73] “Study reveals new physics of how fluids flow in porous media | MIT Energy Initiative.” [Online]. Available: http://energy.mit.edu/news/study-reveals-new-physics-fluids-flow-porous-media/. [Accessed: 04-Aug-2019].

[74] M. L. Brusseau, A. El Ouni, J. B. Araujo, and H. Zhong, “NOVEL METHODS FOR MEASURING AIR-WATER INTERFACIAL AREA IN UNSATURATED POROUS MEDIA,” *Chemosphere*, vol. 127, p. 208, 2015.

[75] F. M. White, *Viscous Fluid Flow, second ed.* 1991.

[76] V. Kumar, C. K. Harris, A. Bronson, S. Shantha-Kumar, and A. Medina, “High-Temperature Liquid Metal Infusion Considering Surface Tension-Viscosity Dissipation,” *Metall. Mater. Trans. B Process Metall. Mater. Process. Sci.*, vol. 47, no. 1, pp. 108–115, 2016.

[77] A. K. Chattopadhyay, “Next Generation Exascale Capable Software for High Fidelity Physics Aware Simulations,” *ETD Collect. Univ. Texas, El Paso*, Jan. 2017.

CURRICULUM VITA

Shaikh Tanveer Hossain earned his bachelor's degree in Mechanical Engineering from Khulna University Engineering and Technology, Bangladesh in 2015. He worked as a plastic product designing and molding engineer at Pran RFL Company in Bangladesh in 2016.

In fall 2016, Tanveer joined the master's program in the Computational Science at The University of Texas at El Paso (UTEP). He worked as a teaching assistant/assistant instructor during his graduate studies at different Departments like Mechanical Engineering, Mathematics at UTEP. He presented his research in a research symposium arranged by UTEP and presented posters and oral presentations in UTEP+NMSU workshop. He mentored several undergraduate students in his time at UTEP. He has published one of his research works in 4th Joint US-European Fluids Engineering Division Summer Meeting of the American society of mechanical engineers (FEDSM2017 ASME)

Tanveer's dissertation work entitled "Numerical Investigation of Molten Metal Infiltration and Pillared Cooling Systems At Microscale'' was supervised by Dr. Vinod Kumar at UTEP. Tanveer looks forward to obtaining a Ph.D. in computational science in future.

Contact email: shaikh.tanveer.hossain@gmail.com

This dissertation was typed by the author.